Predicting pathogen-specific CD8 T cell immune responses from a modeling approach.

Fabien Crauste, Emmanuelle Terry, I Le Mercier, Julien Mafille, Sophie Djebali, Thibault Andrieu, Brigitte Mercier, Gaël Kaneko, C Arpin, Jacqueline Marvel, et al.

Predicting Pathogen-Specific CD8 T Cell Immune Responses from a Modeling Approach[1]

F. Crauste[1,2,*,†], E. Terry[1,2,*], I. Le Mercier[3], J. Mafille[3], S. Djebali[3],T. Andrieu[3], B. Mercier[3], G. Kaneko[5,6], C. Arpin[3], J. Marvel[3], O. Gandrillon[2,5,†]

[1] Université de Lyon, Université Lyon 1, CNRS UMR 5208, Institut Camille Jordan
43 blvd du 11 novembre 1918, F-69622 Villeurbanne-Cedex, France
[2] Inria Team Dracula, Inria Center Grenoble Rhône-Alpes, France
[3] CIRI, INSERM U1111, CNRS UMR 5308; Université Lyon 1, UMS3444/US8;
ENS de Lyon, Université de Lyon, 21 Avenue Tony Garnier, F-69007 Lyon, France
[4] Université de Lyon, INSA-Lyon, INRIA, Laboratoire d'InfoRmatique en Image et Systèmes d'information (LIRIS), CNRS UMR5205, F-69621 Lyon, France
[5] Université de Lyon, Université Lyon 1, CNRS UMR 5534, Centre de Génétique et de Physiologie Moléculaire et Cellulaire, F-69622 Villeurbanne-Cedex, France

† Corresponding authors
* Equal contributors

Abstract

The primary CD8 T cell immune response constitutes a major mechanism to fight an infection by intra-cellular pathogens. We aim at assessing whether pathogen-specific dynamical parameters of the CD8 T cell response can be identified, based on measurements of CD8 T cell counts, using a modeling approach.

We generated experimental data consisting in CD8 T cell counts kinetics during the response to three different live intra-cellular pathogens: two viruses (influenza, vaccinia) injected intranasally, and one bacteria (Listeria monocytogenes) injected intravenously. All pathogens harbor the same antigen (NP68), but differ in their interaction with the host. In parallel, we developed a mathematical model describing the evolution of CD8 T cell counts and pathogen amount during an immune response. This model is characterized by 9 parameters and includes relevant feedback controls. The model outputs were compared with the three data series and an exhaustive estimation of the parameter values was performed. By focusing on the ability of the model to fit experimental data and to produce a CD8 T cell population mainly composed of memory cells at the end of the response, critical parameters were identified.

We show that a small number of parameters (2 to 4) define the main features of the CD8 T cell immune response and are characteristic of a given pathogen. Among these parameters, two are related to the effector CD8 T cell mediated control of cell and pathogen death. The parameter associated with memory cell death is shown to play no relevant role during the main phases of the CD8 T cell response, yet it becomes essential when looking at the predictions of the model several months after the infection.

Keywords: CD8 T Cells ; Immune Response ; Nonlinear Model ; Parameter Value Estimation ; Predictive Model

---

1 Introduction

The adaptative immune response constitutes one of the major mechanisms to fight infection by a pathogen. It involves a wealth of different cell types including B cells, CD4 and CD8 T cells and antigen presenting cells such as dendritic cells. Here, we focus on the cytolytic response mediated by CD8 T cells. These cells play an essential role in controlling infections by intra-cellular pathogens such as influenza viruses (Flu) [1, 2, 3], vaccinia virus (VV) [4, 5] or the bacteria *Listeria monocytogenes* (*Lm*)[6].

We are interested in the specific dynamical behavior of CD8 T cells responding to an infection by an intra-cellular pathogen [7]. After pathogen encounter, CD8 T cells are activated and leave the naive state to enter an expansion phase associated with strong proliferation and differentiation into effector cells. Effector CD8 T cells display cytotoxic capacities that allow them to kill infected cells and clear the pathogen. After the peak of proliferation concluding the expansion phase, most of the population dies by apoptosis in a contraction phase. Effector cells can differentiate into memory cells, a crucial subpopulation able to respond more efficiently and to better control the pathogen in the case of a subsequent infection.

Different models, mainly based upon systems of ordinary differential equations, were proposed to model the details of these cell dynamics kinetics [8, 9, 10]. Antia et al. [11, 12] proposed a model with an age structure for the effector cell equation. They modeled a programmed proliferative response of the CD8 T cells after a pathogen encounter, according to the fact that even with a brief pathogen encounter, a complete response is initiated. They considered a limit age, such that effector cells differentiate into memory cells when they reach this age, provided that they did not die before. No nonlinear dependency of the different rates is considered, only cell age is assumed to act on effector cell proliferation and differentiation, even in the absence of data supporting this assumption.

Inspired by this model, we developed a model [13] of the primary response to an acute infection (when the pathogen has never been encountered before and it does not lead to a chronic infection). Instead of considering an age-dependent regulation of T-cell dynamics, nonlinearities account for feedback controls able to regulate cell dynamics. These controls describe real biological influences of a cell population on differentiation, proliferation and death of the other populations, and on its own fate. For instance, the pathogen amount can induce naive cell activation and differentiation in effector cells [14], as well as proliferation of effector cells [10, 14, 15]. These mechanisms influence the kinetics of the expansion and contraction phases and the switch between these two stages of the response.

In this previous work, several alternative models have been investigated and we ended with the simplest model able to reproduce the CD8 T cell dynamics during a primary response (see [13]). Indeed, simulations were performed to qualitatively reproduce the data found in the literature [7] and the model was able to fit correctly the phases of a primary response to a lymphocytic choriomeningitis virus (LCMV) infection in mice [13]. Those simulations were only performed to qualitatively reproduce a "typical" CD8 T cell immune response, without going any further into a *bona fide* parameter analysis to investigate which values were able to really reproduce relevant kinetics of the response. Furthermore, viral load and virus replication were not considered, whereas they represent key parameters during an infection [16, 17]. Hence, to obtain a more realistic and versatile model that can describe CD8 T cell responses to different pathogens, this infectious process must be taken into account. In this work, pathogen replication is therefore introduced into the model.

Here, this modified model is compared to experimental data that were specifically generated for the purpose of identifying parameter values specific of a given pathogen and of the CD8 T cell response to this pathogen. These data consist in CD8 T cell numbers, measured during the CD8

T cell immune response to three different live intra-cellular pathogens (two viruses: an H1N1 Flu and the Western Reserve (WR) strain of VV; and one bacteria Lm). The three pathogens have been modified by reverse genetics to express the NP68 epitope that is recognized by the F5 T cell receptor (TCR). Hence, we can use transgenic naive CD8 T cells expressing the F5 TCR to monitor the response induced by these 3 different pathogens (H1N1-NP, VV-NP and Lm-NP). Although these pathogens all activate a robust CD8 T cell response, they differ in their interaction with the host in terms of host cells targeted, replication mechanisms and activation of the innate immune response.

Vaccinia virus infection provides protection against variola virus, the causative agent of smallpox, and stands as the classic example of a successful vaccine that confers life long protection. Vaccinia virus, an orthopoxvirus, is a large virus with a double-stranded DNA genome that replicates in the cytoplasm. The WR strain of vaccinia used in this study is a vaccinal strain that was adapted to the mouse [18]. Despite their importance, T cell mechanisms involved in a vaccinia infection were not thoroughly studied [4]. However, smallpox vaccines could be improved, since the existing vaccines are based on live viruses and stay contraindicated for some people [19, 20, 21]. Moreover vaccinia virus could also be used as a platform for the design of vaccines directed against other pathogens [4].

Listeria monocytogenes, a Gram-positive bacteria, causes disease mainly in immunocompromised humans. Humans are exposed to Lm by ingesting contaminated foods such as dairy products. Lm bacteria invade epithelial cells where they replicate. In mice, most studies of infection with Lm focus on immune responses to systemic infection following intravenous inoculation [22]. The highly virulent 10403s strain was used in this study.

Influenza viruses are causative agents of acute respiratory diseases. Influenza is an Orthomyxoviridae with a negative single-stranded RNA segmented genome that replicates in the nucleus. The WSN mouse adapted H1N1 strain was used in this study. Even more than vaccinia, influenza proves to be a topical problem, with the 2009's H1N1 pandemia for example.

Influenza dynamics have been modeled quite extensively (see [23] and [24]). First, influenza infection at population scale was widely studied, to model the spread of the infection by transmission between infected hosts [16, 25, 26, 27, 28, 29, 30, 31, 32]. Second, since the immune response by cytotoxic T cells plays a key role in the evolution of an influenza virus infection [1], immune cell dynamics have been added to models of uninfected/infected cells [33, 34, 35, 36]. In most of these models, an equation was used to describe the immune response, and the T cells were just labelled as activated or cytotoxic, without any further detail. Other authors decided to deal with many cell types involved in the immune response, such as effector cells, antigen presenting cells, B cells and Th1 and Th2 lymphocytes [26, 37]. Yet, none of these models describe the naive, effector and memory states of the CD8 T cell population, or the possible crossregulations and feedback controls between these differentiation stages.

Lee et al. [17] distinguished naive and effector CD8 T cells, but at the cost of an hypersophistication of the model which incorporates CD4 T cells in different states (naive, effector, mature...), B cells, dendritic cells, and uninfected and infected cells. The recirculation of these cells between different organs where the immune response takes place was also modeled. It resulted in a 48 parameter model, that could not be submitted to a systematic parameter sweep. For influenza, many previously described works compared their model to data. To do so, authors estimated part of their parameters and/or used parameters from previously published models or published experimental data [26, 29, 37, 17, 34, 35, 32]. Nevertheless, data used were very heterogeneous and parameter values which were chosen remain difficult to validate, in the absence of a systematic parameter sweep [24] and a lack of identifiability of the models. In addition, these models did not always consider the dynamics of the different CD8 T cell differentiation states involved in the response to influenza.

In the present work, we aim to confront a model describing the mechanisms of a CD8 T cell
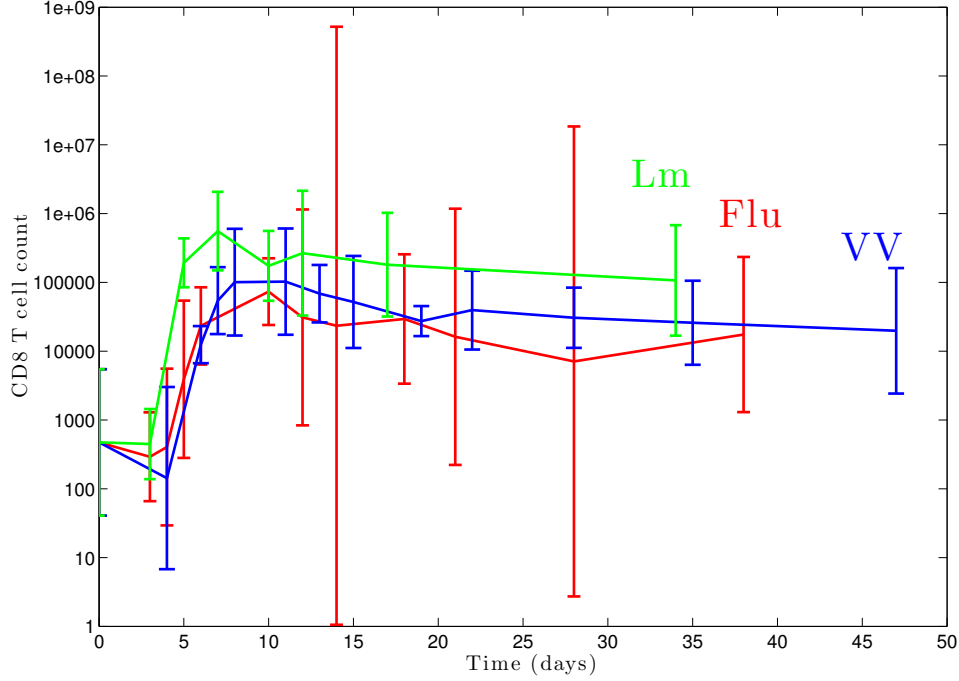
Figure 1: **Experimental data: F5 CD8 T cell counts in the blood for Flu-NP (red) and VV-NP (blue) viral infections and *Lm*-NP (green) bacterial infection.** Each data point corresponds to the mean and standard deviation of CD8 T cell numbers from 5 individual mice.

immune response against infection by an intra-cellular pathogen to experimental data on three different live intra-cellular pathogens, in order to determine relevant parameter values of the model characterizing both the nature of the pathogen (either viruses or a bacterium) and the CD8 T cell response against the NP68 epitope expressed by all three pathogens. To do so, we consider naive, effector and memory differentiation states which were not described in previous models with uninfected/infected cells [33, 34, 35, 36]. Due to the non-identifiability of the parameters, we perform an exhaustive estimation of the model parameter values by comparing the model solutions, obtained with a large range of parameter values, with influenza, vaccinia and *Listeria* experimental data. This allows to determine not one best parameter value which provides a good estimation of experimental data, but a set of values which are suitable for and characteristic of a given parameter. Hence, the role of each parameter – and its associated values – in reproducing a CD8 T cell response against a given pathogen can be evaluated. Values obtained for some parameters are compared with values from the literature and we conclude that our results are coherent with previous studies. We then identify parameters and parameter values that appear to be specific of each infection model, by focusing on the ability of the system to reproduce the main features of a CD8 T cell immune response. Next, we focus on the number of memory CD8 T cells predicted by the model several months after the infection, and determine that a description of memory-cell-dynamics is essential to get a robust and predictive model.
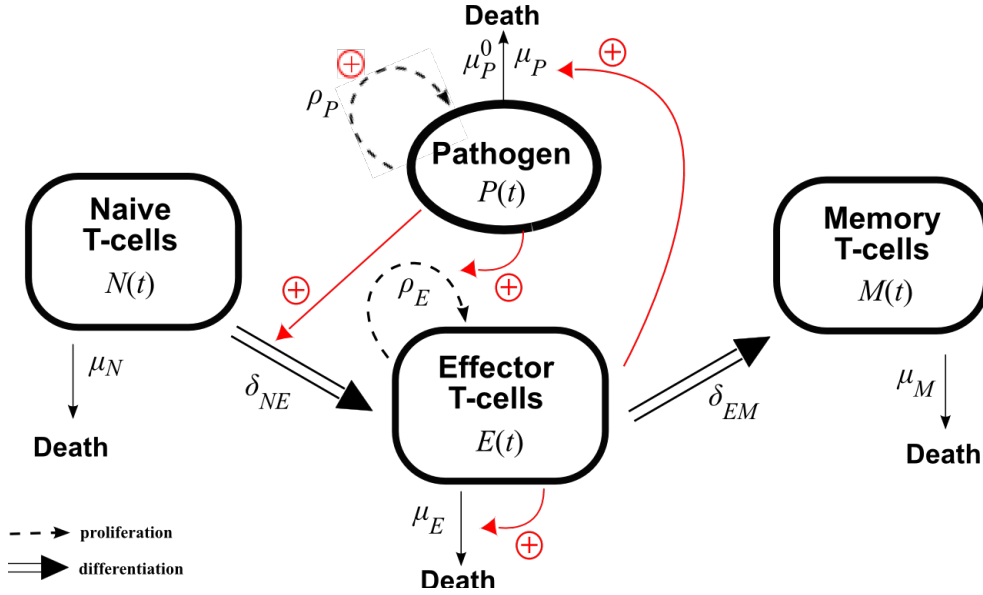
Figure 2: **Schematic representation of the CD8 T cell immune response mechanisms after an infection by an intra-cellular pathogen, either influenza or vaccinia viruses, or *Listeria* bacteria.** Biological justifications of this scheme are mentioned in Section "Model" in Materials and Methods.

2 Results and Discussion

2.1 Data and Best Results

Five measurements of F5 CD8 T cell counts were performed on different time points after infection with influenza, vaccinia or *Listeria* (Section 4.1). The Shapiro-Wilk normality test using a Bonferroni correction showed that experimental data associated with Flu infection are not normally distributed, the hypothesis of a normal distribution on day 14 post-infection being rejected with a *p-value*=0.001. However, the same test showed that experimental data are log-normally distributed. In vivo experimental responses are then presented on Figure 1, using logarithms of the geometrical means of CD8 T cell counts of five mice with the associated standard deviations.

For each data series, a typical qualitative behavior of a CD8 T cell immune response can be observed, with a strong expansion from days 3-4 post-infection, a peak of response which occurs on day 7 post-infection for *Listeria* infection, and around day 10 for influenza and vaccinia infections. The expansion phase is followed by a contraction phase until day 20 post-infection, and a stabilization of CD8 T cell population counts above the initial naive value. Influenza and vaccinia data lead to similar responses, whereas the CD8 T cell response against *Listeria* is characterized by an earlier and stronger proliferation of CD8 T cells. Indeed, the peak for the response to *Listeria* infection reaches around 6×10^5 cells on day 7 post-infection while the peak does not overtake 2×10^5 cells for other infections and occurs between days 8-10 post-infection. This suggests that the class of pathogen and/or the route of inoculation induce different profiles of CD8 T cell responses.

The CD8 T cell immune response against each of the three pathogens was modeled as presented in Figure 2. This model is characterized by 9 parameters (see Section 4.2), which are not identifiable (see Section 4.3 and [38]). Consequently, it is not possible to uniquely identify a parameter value set that would reproduce experimental data. In order to estimate parameter values, a systematic

parameter sweep has been performed. Several values have then been tested for every parameter, and simulations of the model have been compared to experimental data: first to influenza data, followed by vaccinia and *Listeria* data (see Section 4.4). Differences between experimental data and simulations have been measured using a classical criterion of fit quality (minimisation of the weighted residual sum of squares, see Section 4.4).

The best result, for every infection, corresponds to the parameter value set associated with the smallest error value (weighted RSS, see Section 4.4, which equal 2.1 for influenza experiment, 3.6 for vaccinia experiment, and 2.45 for *Listeria* experiment). The best results together with the associated parameter values are presented in Table 1. Correct reproduction of total CD8 T cell count is obtained for the different data series, showing the expected phases of expansion and contraction with a correct quantitative behavior.

These results display a strong fall of cell counts to very low values following the infection. Yet, such falls to low cell numbers between day 0 and day 3 or 4 (which are both equally well fitted, whatever the pathogen) could not be resolved experimentally due to a detection limit around 100 cells.

Parameter values obtained in Table 1 were compared with parameter values available in the literature [8, 39, 40, 41], for models of CD8 T cell immune responses (see Table 2), and results show a correct agreement (same order) between all values. The models used in the literature were confronted to experimental data of LCMV infection in mice. In each model, parameter values were either fixed (using previous data) or estimated. It must be noted first that all these models are linear and do not describe any feedback mechanism controlling cell behavior, and second that not all the parameters used in our model were described in previous modeling efforts, consequently it is not possible to find equivalents of all of our parameters in the literature.

Parameter values obtained for the effector cell proliferation rate in the literature range between 2 and 3 d^{-1}, which corresponds to high values of the non-constant proliferation rate ($\rho_E P$) estimated in this work, whatever the pathogen. Regarding differentiation of effector cells into memory cells, parameter values obtained in the literature range in $[0.004; 0.05]$ d^{-1}. The value preferentially chosen in our analysis is 0.1 d^{-1}, which is slightly larger. All these parameter values are however in the same order and coherent, allowing to be confident in our results.

The value of the parameter describing death of memory cells has not been estimated in previous published papers, instead it has been set either to 0 (assuming no memory cell death) or to 10^{-5} d^{-1}. These values lead to think that death of CD8 memory T cells is unlikely to occur and then it can be unnecessary to include memory cell death in a model of the CD8 immune response. However, since a slow decrease of cell counts is observed in experiments during the memory phase of the three responses (Figure 1), we assumed that even though memory cell death was slow it could be observed during the duration of the experiment (and consequently on a longer term) and then could potentially influence the dynamics of the response. We chose to consider that memory cells had a nonnegative death rate and we tested a large range of values, including the values used in the literature: from $\mu_M = 0$ to $\mu_M = 0.1$ d^{-1}. Whatever the pathogen, no tested value appeared to be preferentially chosen in our analysis (see Figure 4 and Section 2.2).

In the next section, we broaden the scope of our study by focusing on the contribution of each parameter to the response, as a consequence of the systematic investigation of parameter values.

2.2   Contribution of Each Parameter to the Response

A systematic investigation of parameter values allows not only to select values preferentially chosen in the best results for many parameters, but also to get information on the influence of parameters without a priori assumptions. We investigated the frequency of appearance of each tested parameter

Table 1: **Best results for the three experiments and the corresponding estimated parameter values.** Each graph displays the total simulated CD8 T cell count (in black) and experimental data with standard deviation (in red) over the duration (in days) of each experiment. By keeping in mind that for a population $y(t)$ characterized by a growth rate k (which can be either positive or negative) one gets $y(t) = y(0)\exp(kt)$, so for instance $y(t = 1\text{ d}) = y(0)\exp(k)$, then the value $\delta_{NE} = 0.1\text{ d}^{-1}$ (respectively 0.01 and 10^{-3} d^{-1}) corresponds to a differentiation of 10% (respectively 1% and 0.1%) of naive cells into effector cells per day. The same holds for $\delta_{EM} = 0.1\text{ d}^{-1}$: 1% of effector cells differentiate into memory cells per day. The value $\mu_P^0 = 0.1$ d^{-1} (respectively 0.01 and 5.10^{-3} d^{-1}) corresponds to a natural loss of 10% (respectively 1% and 0.5%) of pathogen per day. The values $\mu_N = 1$ and 5 correspond respectively to a death of 65% and 99.5% of naive cells per day. The values $\mu_M = 0.01$ and 0.1 d^{-1} correspond respectively to a loss of 1% and 10% of memory cells per day. *Warning:* parameters ρ_E, ρ_P, μ_E and μ_P do not directly correspond to biological rates (see Supp. Table 2), and their biological meaning is more difficult to define. Confidence intervals appear below each parameter value.
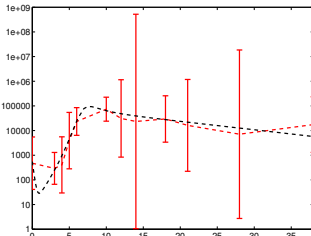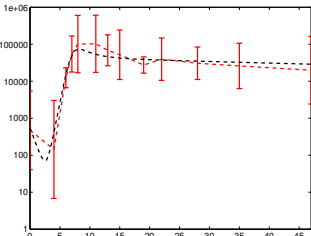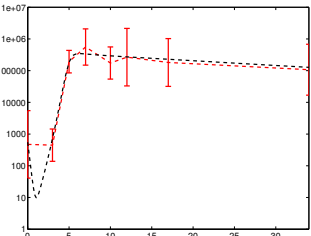
Parameter values	Influenza infection	Vaccinia infection	*Listeria* infection
μ_N (d^{-1})	5 (3.78;6.22)	1 (0;2.51)	5 (2.7;7.3)
δ_{NE} (d^{-1})	0.1 (0.09;0.11)	10^{-3} (0;0.02)	0.01 (0;0.02)
ρ_E (d^{-1})	1 (0.77;1.23)	2 (1.61;2.39)	2 (1.62;2.37)
μ_E	10^{-5} (0;2.4×10^{-5})	10^{-5} (0;2.8×10^{-5})	10^{-5} (7.6×10^{-6};1.2×10^{-5})
δ_{EM} (d^{-1})	0.1 (0.09;1.11)	0.1 (0.09;0.11)	0.1 (0.08;0.12)
μ_M (d^{-1})	0.1 (0.88;1.12)	0.01 (0;0.02)	0.1 (0.08;0.12)
ρ_P (d^{-1})	0.1 (0.09;0.11)	0.1 (0.06;0.14)	0.1 (0.07;0.13)
μ_P	10^{-5} (0;2.4×10^{-5})	10^{-5} (0;2.9×10^{-5})	10^{-6} (0;3.6×10^{-6})
μ_P^0 (d^{-1})	0.01 (0;0.24)	0.1 (0.08;0.12)	5.10^{-3} (0;0.02)

Table 2: **Comparison between parameter values from the literature and the best parameter values of this paper's model**. The upper part of the Table gives estimations of some parameter values characterizing the CD8 T cell immune response (proliferation and differentiation rates of effector cells, and death rate of memory cells) obtained from 4 manuscripts published between 2001 and 2007 [8, 39, 40, 41]. Values in red (all the memory cell death rate values, and two values of proliferation rates) were a priori fixed in these works and not estimated. The bottom part of the Table gathers estimations of parameter values from our analysis, using the parameter values giving the best comparison to experimental data (see Table 1). In particular, one must note that in our case the proliferation rate of effector cells is non-constant and pathogen count-dependent (it equals $\rho_E P(t)$), so the parameter ρ_E is not the proliferation rate. We then indicate ranges of variations for the proliferation rate of effector CD8 T cells. The * in the pathogen column indicates a chronic infection. All other infections are acute.

Reference	Effector cell prol. rate (d^{-1})	Effector cell diff. rate (d^{-1})	Memory cell death rate (d^{-1})	Pathogen
De Boer et al. [8] NP118 epitope	2.9	0.011	10^{-5}	LCMV
De Boer et al. [8] GP283 epitope	2.6	0.014	10^{-5}	LCMV
De Boer et al. [39]	1.9	0.018	0	LCMV
Althaus et al. [40]	1.9	0.004	0	LCMV
Althaus et al. [40]	1.9	$0.02 - 0.05$	0	LCMV*
Ganusov et al. [41]	1.99	0.02	0	LCMV
This Paper's Model	$0.02 - 1.9$ $0.001 - 2$ $0.58 - 3.6$	0.1 0.1 0.1	0.1 0.01 0.1	Flu-NP VV-NP Lm-NP

value, in the parameter value sets corresponding to the acceptable sets (see Section 4.4). It corresponds to approximately 97,000 parameter value sets for Flu infection, 51,000 for VV infection, and 6,400 for Lm infection, for which all simulations of CD8 T cell kinetics are in good, or very good agreement with experimental data.

Three groups of parameters emerged: a first group is characterized by parameters (ρ_E, μ_E, μ_P) with constrained values; a second group is characterized by pathogen-independent values for each parameter $(\delta_{EM}, \mu_P^0, \mu_M)$; the third group is composed of parameters $(\rho_P, \mu_N$ and $\delta_{NE})$ exhibiting differences between values selected for *Listeria* infection on one hand and influenza and vaccinia infections on the other hand.

First, independently of the pathogen, values of parameters ρ_E for the effector cell proliferation, μ_E for the effector cell-dependent effector cell death rate, and μ_P for the effector cell-dependent pathogen death rate appear to be constrained in the set of acceptable parameter values (Figure 3). In addition, the preferentially selected values depend on the nature of the pathogen, with differences observed between responses to viral infections and to Lm infection. Indeed, the values $\rho_E = 1.5$,
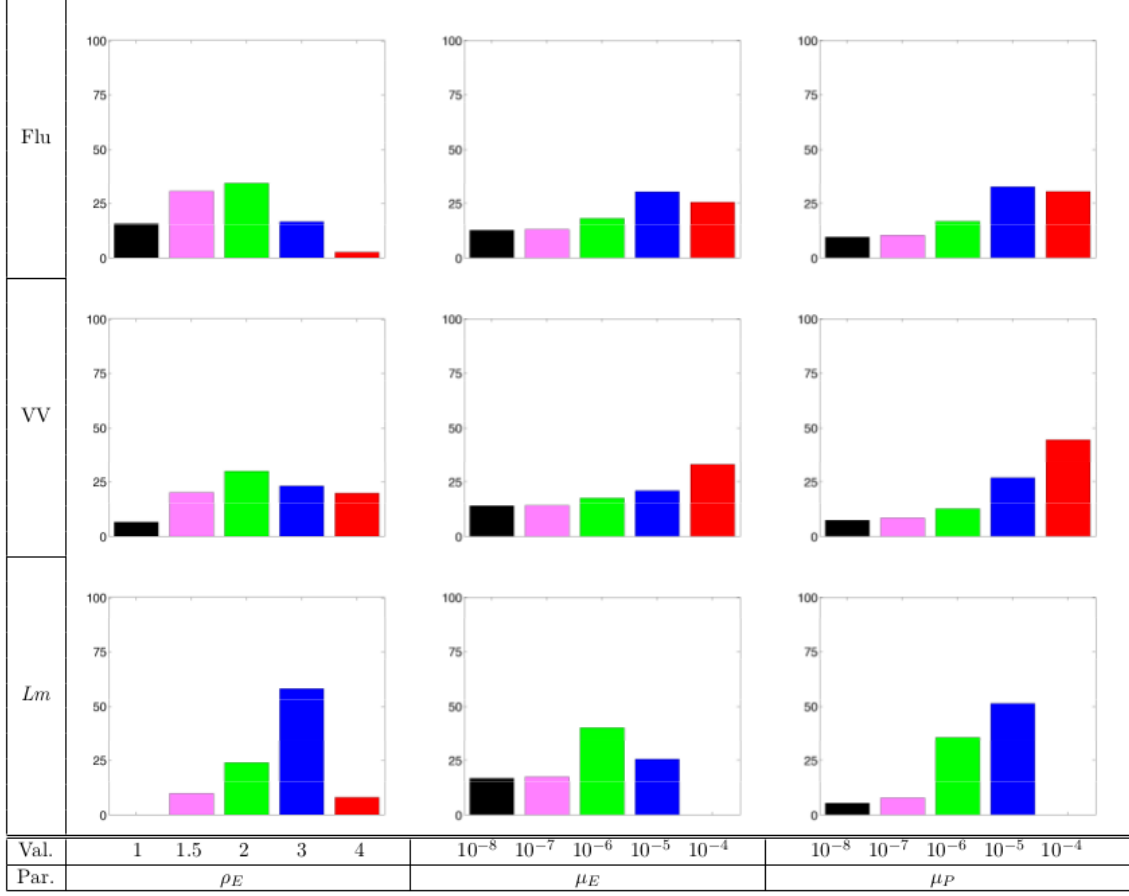
Figure 3: **Frequency of appearance of tested parameter values for ρ_E, μ_E, and μ_P.** Each bar in histograms corresponds to a percentage of appearance of a parameter value within the acceptable parameter value sets, and the sum of the 5 values of each histogram always equals 100%. For each parameter, the 5 tested values are indicated below the corresponding bars.

2 and 3 d^{-1} represent 80% and 75%, respectively, of selected values for influenza and vaccinia infections, and the values $\rho_E = 2$ and 3 d^{-1} represent 80% of selected values for *Listeria* infection. The same proportions are observed for the values $\mu_E = 10^{-6}$, 10^{-5} and 10^{-4} cell^{-1}.d^{-1} for influenza and vaccinia infections, and $\mu_E = 10^{-7}$, 10^{-6} and 10^{-5} cell^{-1}.d^{-1} for *Listeria* infection. Regarding the parameter μ_P, values $\mu_P = 10^{-6}$, 10^{-5} and 10^{-4} cell^{-1}.d^{-1} represent 80% of selected values for influenza infection and 85% for vaccinia infection, whereas the values $\mu_P = 10^{-6}$ and 10^{-5} represent 85% of selected values for *Listeria* infection.

Although distributions seem to be less constrained for influenza and vaccinia infections, with 3 values preferentially expressed compared to 2 values for *Listeria* infection, these first results tend to indicate that the CD8 T cell immune response to an infection by influenza or vaccinia is characterized by lower proliferation rates and higher apoptosis rates of effector cells than a response to an infection by *Listeria*.

Second, the opposite situation is also observed, that is parameters for which there is no relationship between the pathogen and the preferentially chosen values (Figure 4). Parameters δ_{EM}, the differentiation rate of effector cells in memory cells, μ_P^0, the pathogen natural death rate, and μ_M accounting for memory cell death, are in this group of parameters. Values of the parameter
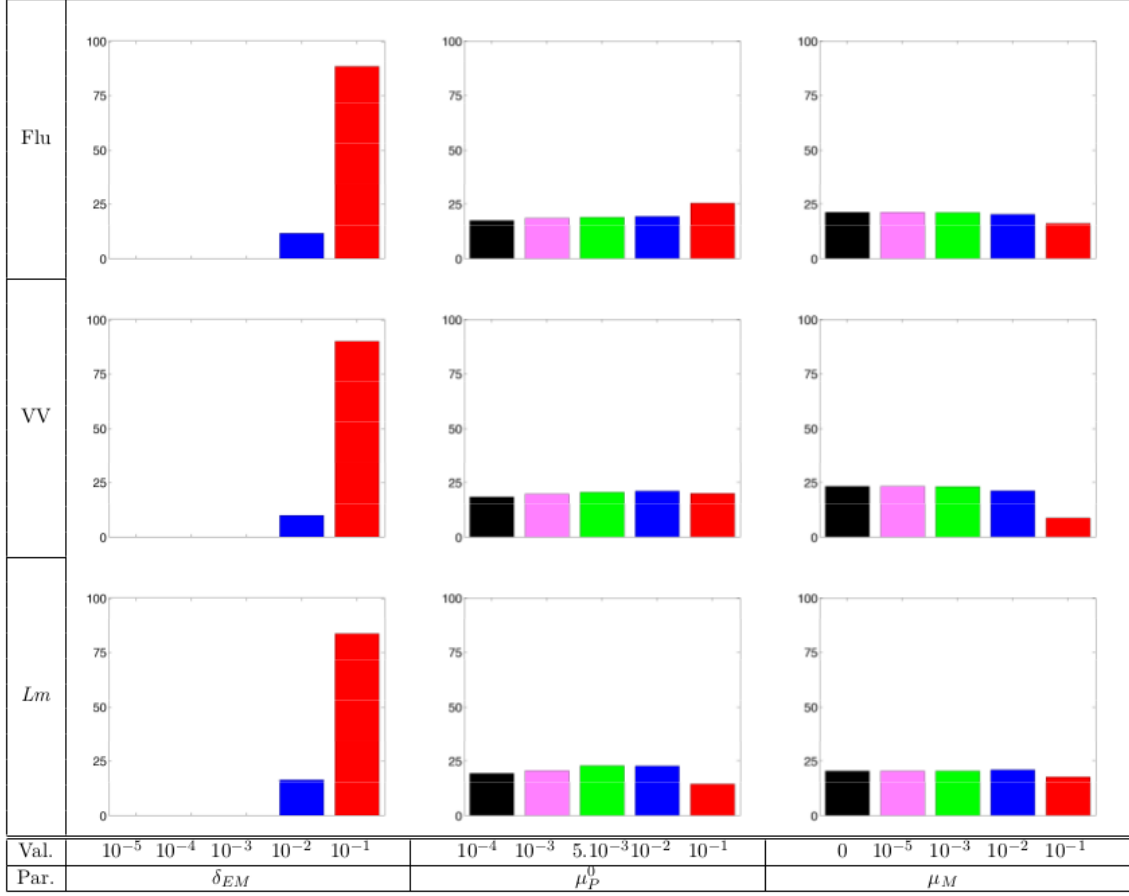
Figure 4: **Frequency of appearance of tested parameter values for δ_{EM}, μ_P^0, and μ_M.** Each bar in histograms corresponds to a percentage of appearance of a parameter value within the acceptable parameter value sets, and the sum of the 5 values of each histogram always equals 100%. For each parameter, the 5 tested values are indicated below the corresponding bars.

δ_{EM} are strongly constrained around high values (between 0.01 and 0.1 d^{-1}), independently of the pathogen. This is due to the fact that we required CD8 T cell populations to be mainly composed of memory cells at the end of the experiment (see Section 4.4). The parameter δ_{EM} appears to be the main contributor to the fast generation of memory cells, whatever the pathogen (see below, section Crossing Times Between Effector and Memory Cell Populations). For μ_P^0 and μ_M the five values are almost uniformly distributed among the acceptable parameter value sets. This includes the value $\mu_M = 0$, indicating that the dynamics of memory cells weakly contributes to the description of the CD8 T cell immune response over the first weeks of the response (all responses were approximately measured over 6 weeks). The t-test and an F-test for equality of two variances show no differences between the three distributions (*p-values*> 0.01, except for the F-test between VV and *Lm* distributions of μ_M where the *p-value*= 0.009).

Both parameters μ_M and δ_{EM} are related to memory cell dynamics, and it can be hypothesized that dynamics of memory cells does not modify the total CD8 T cell dynamics and can be omitted while fitting experimental data on the total CD8 T cell counts, at least for the duration of the experiment. For μ_P^0, one can also observe that all values are almost selected with the same probability, even though a response against Flu infection may have a tendency to select higher values of

μ_P^0 than other responses (no statistical difference with the t-test and the F-test, *p-value*> 0.01). At this stage, this tends to indicate, as a model's prediction, that the CD8 T cell response is mostly independent of the natural death rates of the pathogens.
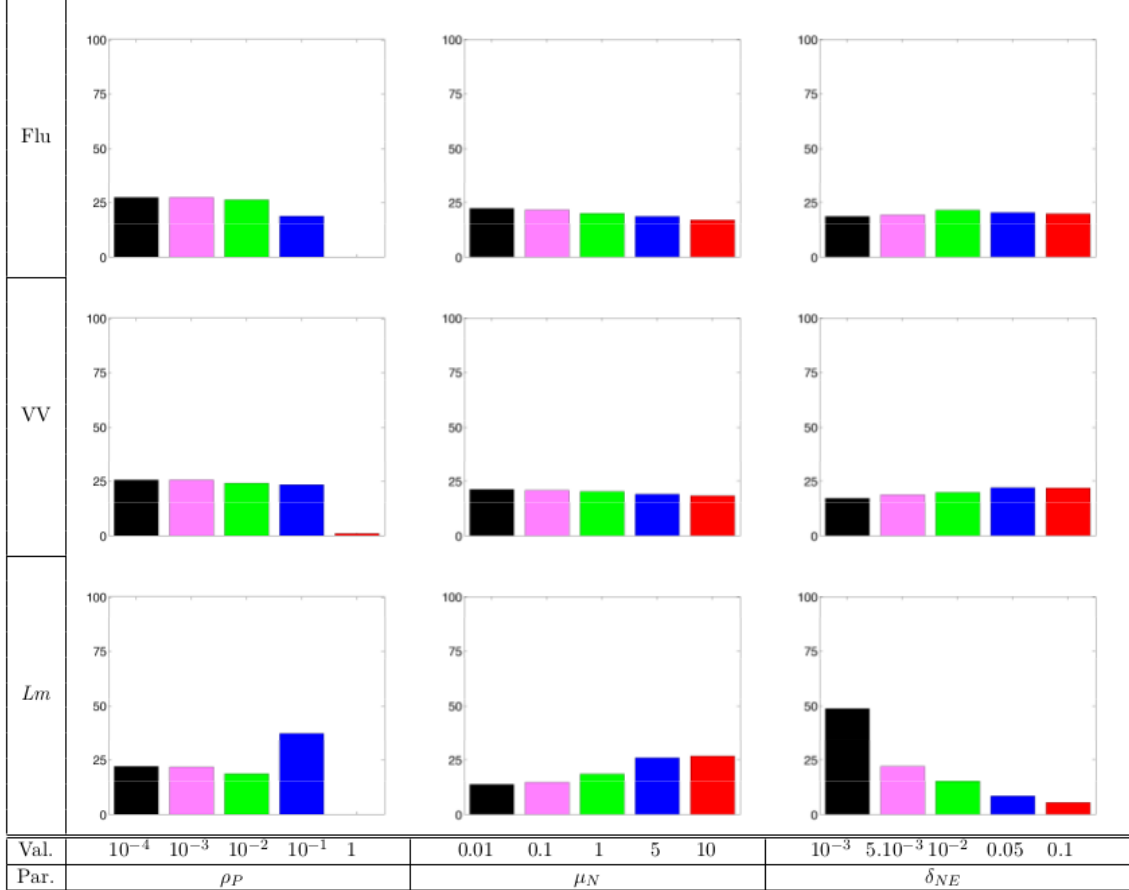

Figure 5: **Frequency of appearance of tested parameter values for ρ_P, μ_N, and δ_{NE}.** Each bar in histograms corresponds to a percentage of appearance of a parameter value within the acceptable parameter value sets, and the sum of the 5 values of each histogram always equals 100%. For each parameter, the 5 tested values are indicated below the corresponding bars.

Then we are left with 3 parameters, ρ_P, μ_N, and δ_{NE} (Figure 5), for which distributions of parameter values are not constrained (compared to the first group, see Figure 3), but can individually account for pathogen-specific distributions. As we already observed for parameters in Figure 3, some parameter values can identify a CD8 T cell immune response either against a virus or against bacteria.

Even though no statistical difference is found neither with the t-test nor the F-test between ρ_P distributions, which appear to be similar for all pathogens, average values slightly differ. They equal 0.0044d^{-1}, 0.0073d^{-1}, and 0.08d^{-1} for influenza, vaccinia, and *Listeria* infections, respectively. Since ρ_P characterizes the proliferation of the pathogen, we can hypothesize that proliferation of influenza and vaccinia viruses is slower than the proliferation of *Listeria* bacteria, in this context of an immune response. A similar result has been identified for ρ_E and μ_E, for which selected values were similar for responses against Flu and VV and different from selected values for a response against *Lm* (Figure 3). Interestingly, both the effector cell proliferation rate and the pathogen

11

proliferation rate are functions of pathogen counts, and thus characterized by pathogens dynamics (and as mentioned in the next section, see Figure 7, selected values of these two parameters are strongly correlated). We cannot however exclude that the difference observed for parameters ρ_E and ρ_P may be due to rescaling involving the initial pathogen count (see Section 4.2), which could result in differences between the three infections.

Distributions of parameter values for δ_{NE} exhibit similarities for the immune responses against influenza and vaccinia, with all values almost uniformly selected, whereas the response against *Listeria* infection preferentially selects low values ($\delta_{NE} < 0.01$ d^{-1}). No statistical difference is found neither with the t-test nor the F-test between Flu and VV distributions of δ_{NE}, whereas both tests show significant statistical differences between Lm distributions and the other pathogen distributions for δ_{NE} (*p-values*< 0.001). We could hypothesize that a response against Lm is characterized by a slower conversion rate of naive to effector cells than a response against Flu and VV.

The naive cell death rate μ_N also shows a pathogen-specific distribution with higher values picked up for Lm than for VV and Flu infections. As noticed for δ_{NE}, no statistical difference is found neither with the t-test nor the F-test between Flu and VV distributions of μ_N yet both tests show significant statistical differences between Lm distributions and the other pathogen distributions (*p-values*< 0.001). It is difficult to explain how the pathogens influence the death rate of naive cells, but one can note that for Lm infection this parameter is partly inversely correlated to δ_{NE} and its selectivity may reflect δ_{NE}'s selectivity (see Supp. Fig. 1).

The above analysis suggests that some parameters (ρ_E, μ_E, μ_P, and to some extent ρ_P) could allow to distinguish between a CD8 T cell immune response targeted against a virus infection such as influenza or vaccinia, on one hand, or against a bacteria infection such as *Listeria* on the other hand. It must be noted that what is observed here may not only results from the nature of the pathogens (viruses versus bacteria) but also from the context of the response, e.g. the infection routes.

2.3 Correlated Expressions of Parameter Values

The previously mentioned hypothesis, regarding a higher activation rate of naive cells during influenza and vaccinia infections, has to be modulated. To determine parameter values able to reproduce CD8 T cell kinetics some parameters can be bound by an artificial link: in order to reproduce a key feature (for instance, the initial decrease of the number of CD8 T cells on the first days of the response, or the strong expansion phase few days post-infection), a combination of parameter values can be selected.

During the process of parameter value estimation, interdependencies of parameter values can be observed. Using Pearson's correlation matrices, correlation between two parameters can be measured, for the three experiments. This is illustrated on Figure 6, where the darker the blue the higher the correlation coefficient.

Although for most parameters in the model no correlation with another parameter is observable (in particular, parameters μ_N and μ_M show no correlation with almost all other parameters), some parameters exhibit high correlation coefficients with several parameters. Independently of the considered pathogen, parameter μ_P is strongly correlated with parameters μ_E and δ_{EM}. In addition, for both influenza and *Listeria* infections, parameter ρ_E appears strongly correlated with δ_{NE}, μ_E, ρ_P and μ_P^0. Finally, parameters for which the strongest correlations are measured, throughout the three experiments, are the pairs (μ_E, μ_P), (ρ_E, ρ_P), and (δ_{NE}, ρ_E).

When looking more closely to these three pairs of parameters, one can observe different behaviors. Figure 7 shows the frequencies of appearance of every pair of (μ_E, μ_P) values, for vaccinia and
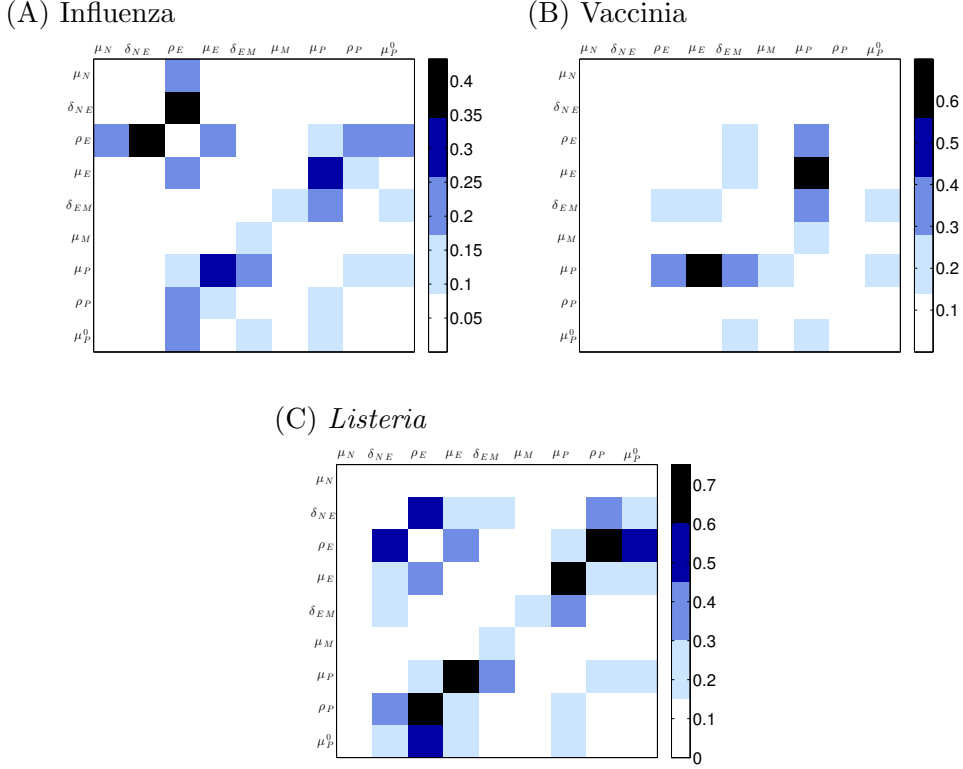
Figure 6: **Pearson's correlation matrices.** For influenza (A), vaccinia (B), and *Listeria* (C) infections, Pearson's correlation coefficients have been computed and represented using a color code: the darker the blue, the more correlated the parameters (white indicates no correlation, except for the diagonal of matrices, which should appear in black (correlation coefficient equal to 1); this color has been avoided for the sake of clarity). Note that all matrices are symmetric, and absolute values of correlation coefficients have been represented.

Listeria experiments, of (ρ_E, ρ_P) values for *Listeria* experiment, and of (δ_{NE}, ρ_E) values for influenza experiment, among the acceptable parameter sets. The height of red vertices indicates the percentage of parameter sets using the associated pair-value. Uncorrelated parameters would be characterized by a similar distribution of parameter values whatever the value of the other parameter (see Supp. Fig. 2). This is clearly not the case for all pairs (although it is less clear for values of (δ_{NE}, ρ_E)) where values of one parameter are strongly associated with one or two values of the other parameter, and for a given parameter value the distribution of values of the other parameter is very different.

High values of μ_E are associated with small values of μ_P and conversely, even though the associated pairs of values depend on the pathogen. Regarding the values of (ρ_E, ρ_P), a similar relationship is observed, high values of one parameter associated with a low value of the other, yet the result is less obvious for Flu and VV (data not shown).

These 4 parameters are associated with the main feedback controls described in the CD8 T cell immune response model: μ_E and μ_P characterize the cytolytic action of effector cells (respectively by fratricidal killing and killing of the pathogen), and ρ_E and ρ_P the proliferation rates of effector cells and of the pathogen, respectively. This stresses the importance of feedback regulation for a correct quantitative behavior of the model but also the emergence of a subtle equilibrium between
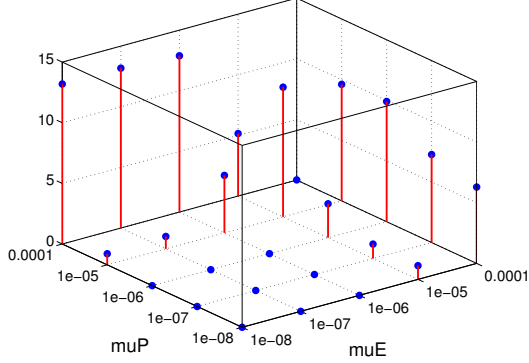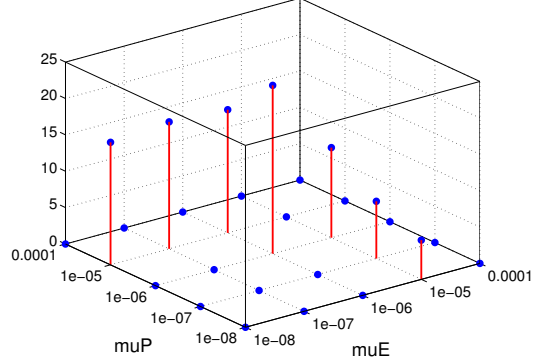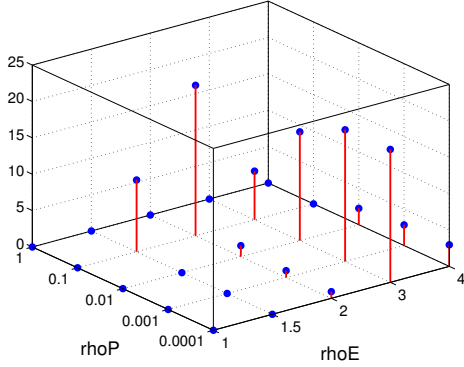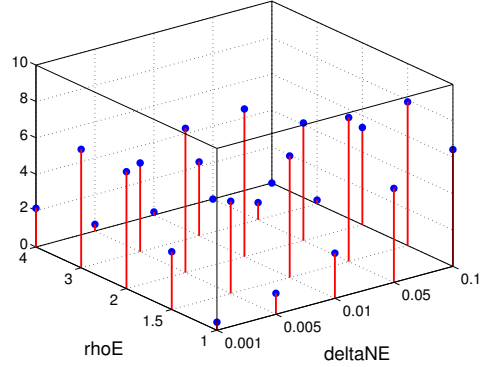
Figure 7: **Frequencies of appearance of values of** (μ_E, μ_P), (ρ_E, ρ_P), **and** (δ_{NE}, ρ_E) **among the acceptable parameter value sets.** For correlated parameters, values of one parameter are strongly associated with one or two values of the other parameter. (A) Values of (μ_E, μ_P) for vaccinia infection. (B) Values of (μ_E, μ_P) for *listeria* infection. (C) Values of (ρ_E, ρ_P) for *Listeria* infection. (D) Values of (δ_{NE}, ρ_E) for influenza infection.

the different feedback processes involved in the regulation of CD8 T cell counts during the acute phase of the response.

Parameters δ_{NE} and ρ_E are related to the activation of the CD8 T cell response: they allow a description of the naive cell population dynamics in association with the presentation of the antigen and the beginning of the expansion phase. For the three pathogens (data not shown), high values of δ_{NE} are preferentially associated with low values of ρ_E, whatever the pathogen. This means that when a lot of naive cells are activated it is not necessary to increase proliferation of the newly created activated cells to reproduce the expansion phase. The two processes (naive cell activation and proliferation of activated cells) are strongly linked, resulting in a correct CD8 T cell dynamics.

Quantitatively, parameters δ_{NE} and ρ_E take different values depending on the pathogen, yet qualitatively they characterize similar behaviors of the CD8 T cells in situations of infections by live pathogens. Selected values allow to correctly describe the first days of the response, including the expansion phase, even if the cost is to over-estimate naive cell loss (by cellular death and differentiation in effector cells), because this can be compensated by an under-estimation of effector cell proliferation rates.

On one hand, infection with influenza or vaccinia virus is characterized by high differentiation rates from naive to effector cells, and by mid-range proliferation rates. On the other hand, a low
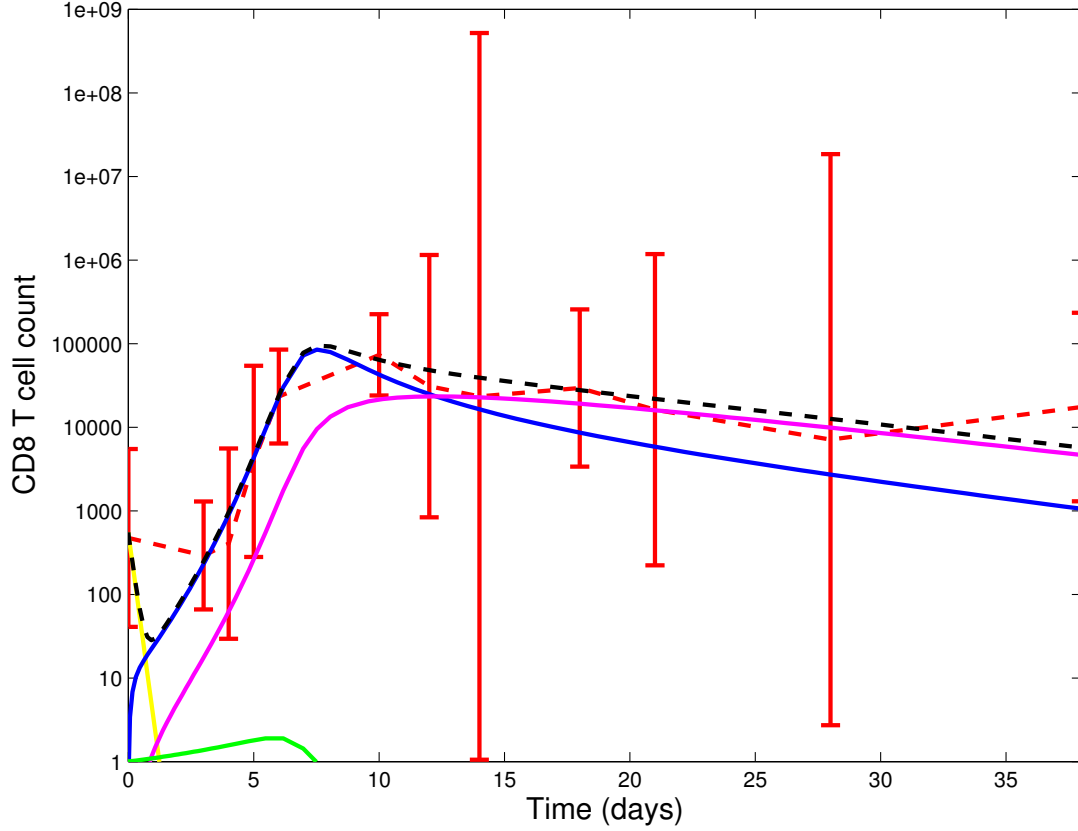
Figure 8: **CD8 T cell subpopulation dynamics on the best result for influenza infection.** Experimental data are given by the red dashed line, with standard deviation, and the total number of CD8 T cells is represented by a dashed black line. Naive cells (yellow straight line), effector cells (blue straight line), memory cells (pink straight line), and pathogen count (green straight line) are also displayed.

differentiation rate from naive to effectors cells and high proliferation rates are associated with infection to *Listeria* bacteria. This makes once again response to *Lm* infection look different than viral infections, in terms of the dynamics of the CD8 T cell response.

2.4 Crossing Times Between Effector and Memory Cell Populations

In every simulation, the experimental number of CD8 T cells is compared (see Section 4.4) to the sum of the three simulated counts of CD8 T cell subpopulations. However, the model has been built to perform an explicit computation of the three subpopulations of naive, effector and memory cells, and it allows to follow their kinetics after the pathogen introduction (see Figure 8). The behavior of these subpopulations can therefore be used for restricting the selected parameter values. Acceptable parameter value sets have been obtained by restricting the sets of parameter values minimizing the Residual Sum of Squares to parameter sets exhibiting a cell population mainly composed of memory cells at the end of the experiment (see Section 4.4).

Distributions of *crossing times* (that is, the time when the memory cell count becomes larger than the effector cell count) are bimodal, with more than 75% of parameter value sets associated with an early crossing (before day 20 post-infection, that is before the end of the contraction phase,
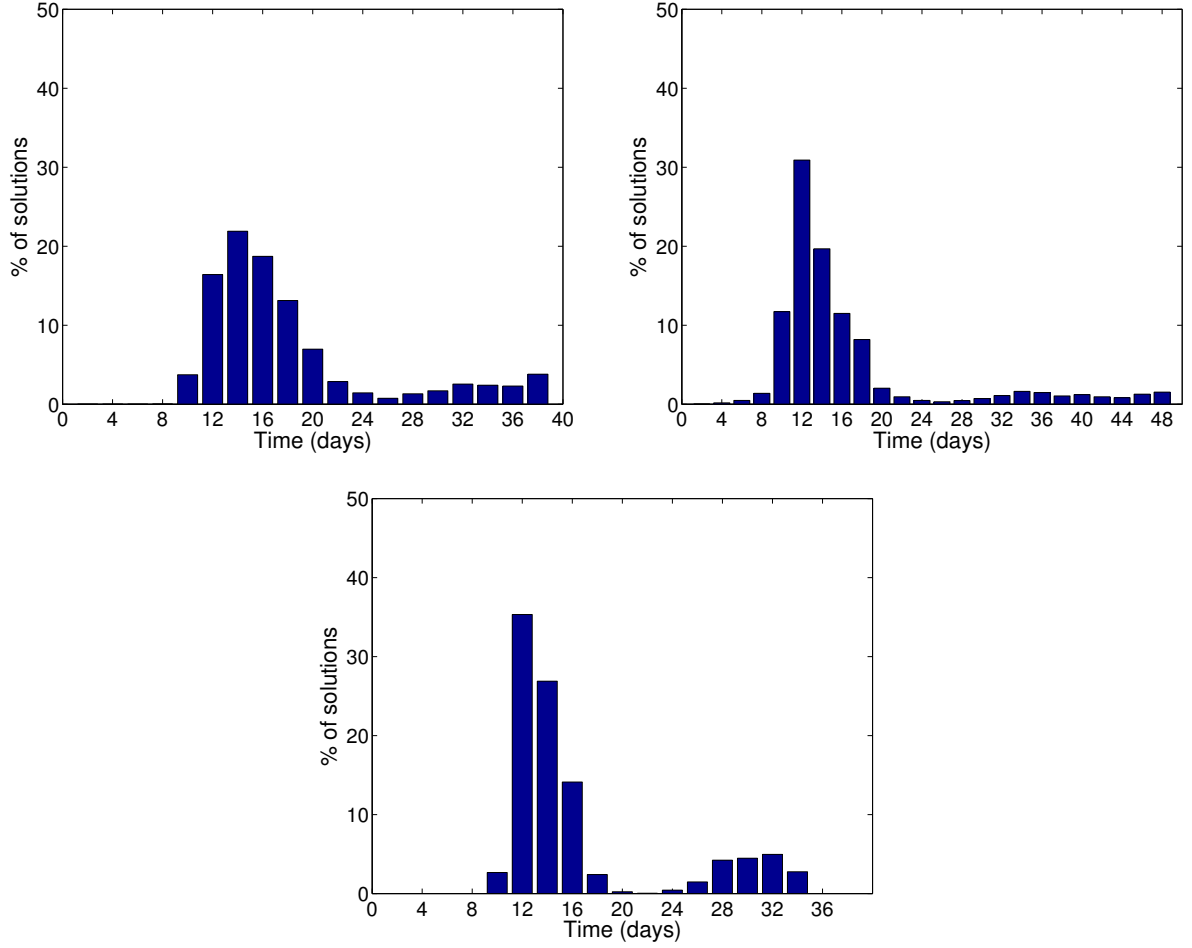
Figure 9: **Distributions of crossing times.** Crossing times are computed for every parameter value set in the acceptable parameter value sets, on the duration of the experiment, for the three pathogens: Flu (top left, $t_{max} = 38$ days), VV (top right, $t_{max} = 47$ days), and Lm (bottom, $t_{max} = 34$ days). Percentages of solutions exhibiting a crossing time are displayed. The sum of bars in each graph equals 100%.

see Figure 1) and the remaining parameter value sets associated with a late crossing of the cell populations (see Figure 9). The rate of differentiation in memory cells, δ_{EM}, is responsible for an early or late crossing. Figure 4 shows the values of δ_{EM} expressed among the best results, which are strongly constrained whatever the pathogen. Additional analyses showed that simulations with a high differentiation rate ($\delta_{EM} = 0.1$ d^{-1}) produce an early crossing, whereas simulations with a lower differentiation rate ($\delta_{EM} = 0.01$ d^{-1}) produce late crossings (data not shown). Hence, the differentiation rate of effector cells appears to be the main contributor to the generation of a CD8 T cell population composed of memory cells at the end of the experiment, and in addition its value influences the speed (early or late crossing) at which memory cells are produced. Only access to experimental data identifying CD8 T cell subsets and counting them at given time points would allow to determine the value of δ_{EM} (see the discussion in Section 3).

2.5 Predicting Memory Cell Quality

The model allows to track subpopulation kinetics on a timescale that extends much further than the experimentally measured points, and can consequently make long term predictions that are testable experimentally on the number of CD8 T cells, or CD8 memory T cells.
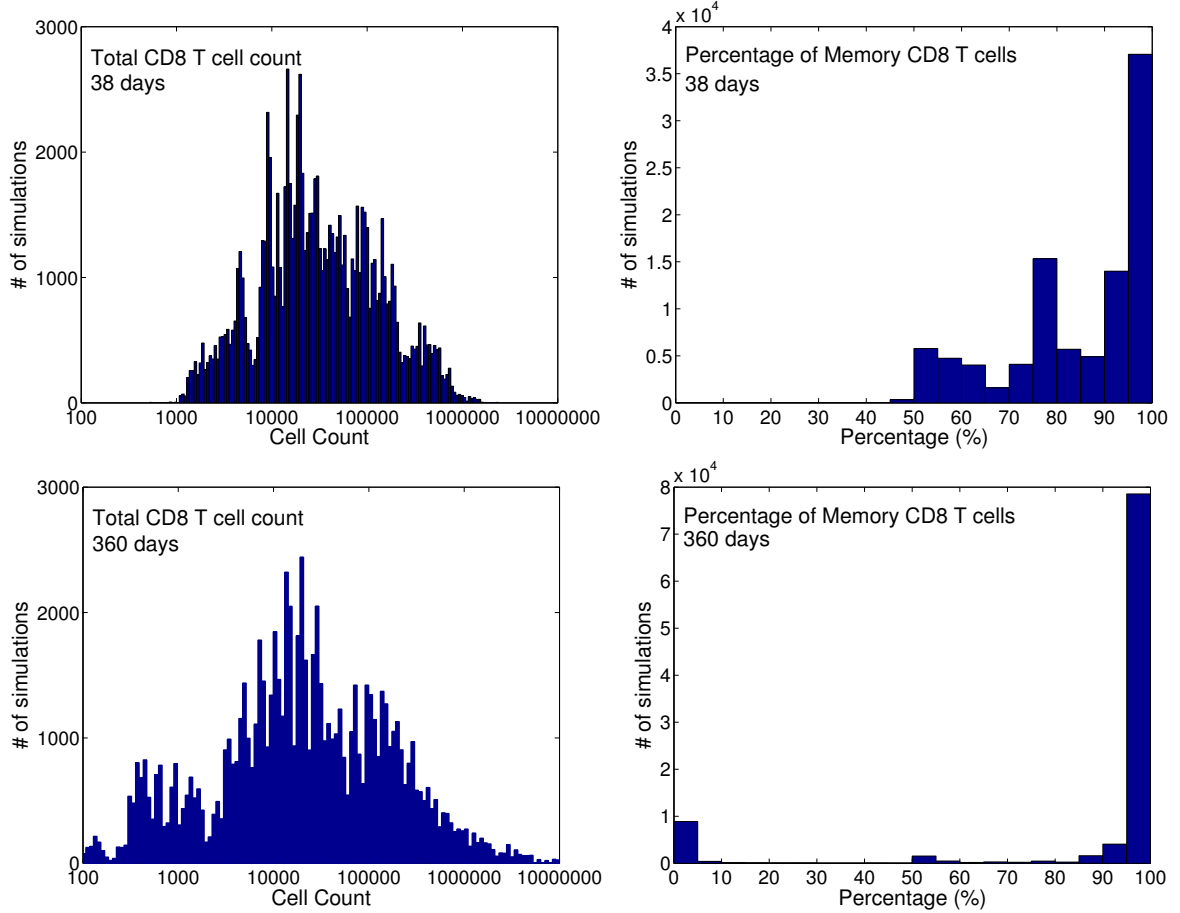

Figure 10: **Total number of CD8 T cell counts and percentages of memory cells among the total CD8 T cell population predicted by the model for Flu infection.** For every parameter value set among the acceptable ones, the histograms of the number of simulations associated with a given count of total CD8 T cells (left panels) and with a given percentage of memory cells among the total CD8 T cell population (right panels) are presented, both at the end of the experiment (D38, top) and at D360 (bottom).

Figure 10 shows the distributions of the total CD8 T cell counts at day 38 post-infection (the end of the experiment) and the predicted values at day 360 post-infection, for Flu experiment (left panel). Differences observed in CD8 T cell counts on day 360 post-infection are mainly due to the value of the memory CD8 T cell death rate μ_M: the lower μ_M the larger the number of CD8 memory T cells on day 360 post-infection.

For the same experiment and on the same days (D38 and D360 post-infection), Figure 10 also shows (right panel) the number of simulations exhibiting a given percentage of memory cells among the total CD8 T cell population. On day 38 post-infection, about 50% of the simulations are

associated with a total CD8 T cell population mainly made of memory cells (more than 90%), with some heterogeneity (some simulations are only composed of 50% of memory cells). The model predicts that at day 360 post-infection the CD8 T cell population is exclusively made of memory cells (more than 95%) for more than 90% of the simulations, as expected, with about 10% of the simulations associated with a low percentage of memory cells in the population (these simulations correspond to a low total CD8 T cell population count). On day 360 post-infection most parameter value sets then predict a sustained memory CD8 T cell population. The same observations are made for infections to VV (Supp. Fig. 3) and *Lm* (Supp. Fig. 4).

Predictions made by the model, in terms of CD8 T cell counts computed for every set of parameter values included in the acceptable parameter value sets, can then allow to validate the model but also to discriminate parameter value sets according to their predictive values on the long term behavior of the system.

3   Conclusion

In the present work, we considered a model of the CD8 T cell immune response describing naive, effector and memory cell subpopulations kinetics, together with pathogen replication. Feedback loops in the model, based on experimentally described biological phenomena, led to realistic mechanisms controlling cell population behavior. We previously demonstrated that this model correctly reproduces a qualitative typical CD8 T cell immune response [13]. In order to explore in finer details the quantitative behavior of our model, we generated specific experimental data to confront the model to different dynamics of CD8 T cell immune responses to three intra-cellular pathogens, two viruses (influenza and vaccinia) and one bacteria (*Listeria*) all harboring the same antigen (NP68).

Parameter value estimation was performed by fitting the model to total CD8 T cell counts generated experimentally. We first focused on the parameter values that gave the best results, which proved to be coherent with values obtained in the literature. Then we showed that among the acceptable parameter value sets, corresponding simulated solutions are similarly able to reproduce the data. Different groups of parameters emerged, characterized by their ability to reproduce the CD8 T cell response to either only one, two, or three pathogens (see Figures 4 and 5 for parameters δ_{EM} and ρ_P, respectively). Between 2 to 4 parameters, specific of the effector CD8 T cell response, and the associated biological processes were identified as responsible for the response towards a given pathogen. We then focused on the memory cell population, and how it can be used to discriminate between parameter value sets. Finally, we investigated the predictions of the model in terms of memory cell counts theoretically observable few weeks or months after the end of the experiment and determined that it depended exclusively on the value of the memory cell mortality rate.

In many previous works dealing with the modeling of the CD8 T cell immune response where models were compared to data [17, 35, 39, 40, 8], only the best parameter value set (and usually a confidence interval) providing a good fit on the data was determined. Due to the non-identifiability of the model's parameters, we decided to provide a larger parameter space exploration, and we performed a systematic parameter sweep. The first consequence has been that a large number of parameter sets proved to be "acceptable", i.e. correctly reproduced quantitatively the data. We have then shown that adding a new biological information (early crossing between memory and effector cell subpopulations, prediction of memory cell count long after the end of the experiment) led to a significant decrease in the number of acceptable parameter value sets. More experimental work is currently ongoing to add more relevant constraints (see below). This approach also allowed us to better estimate the influence of each parameter and to distinguish between sensitive and non-sensitive parameters.

It is worth mentioning that this approach also provides insight into the influence of mice-to-mice biological variability. Although our experiments were performed in a very controlled setting (transgenic cells in congenic animals), the amount of variability is clearly evident (Figure 1). It is therefore highly unlikely that a single parameter value set would fit all the different mice. Our parameter sweep procedure helps therefore capturing part of this biologically relevant variability, since distributions of parameter values are much more realistic for biological processes.

Parameters associated with effector cell death and pathogen clearance, both dependent on the number of effector CD8 T cells (via a feedback control), showed to be the most relevant ones to identify the pathogen responsible for the infection: according to their values, one may be able to determine the nature of the pathogen (see Figure 3). The physiological, and most importantly inflammatory, context of an infection influences the quantity and quality of the generated effector cells [42]; this may translate in different effector-induced death rates and effector proliferation rates in our immunization protocols. We also showed that values of these two parameters are correlated, and better than considering individual values of these parameters one should consider pairs of parameter values. An experimental investigation of CD8 T cell apoptosis along the resolution of the infection, together with an experimental measurement of the pathogen kinetics, should allow determining more precisely parameter values associated with the CD8 T cell immune response (see below).

Secondary parameters have been identified as contributors to the fitness of the model. These parameters are related to effector cell dynamics (effector cell proliferation rate and their rate of differentiation in memory cells). From the selected values of these parameters, one may hypothesize that influenza and vaccinia infections are characterized by low proliferation rates of CD8 effector T cells, compared to *Listeria* infection which is associated with high proliferation rates of CD8 effector T cells (see Figure 3). This could be expected as the level of inflammation not only controls the extent of the expansion phase, but also its duration [42].

On the contrary, the parameter associated with memory cell death showed no relevance in describing the effector CD8 T cell response and the memory phase over 5-6 weeks. Yet, the memory cell death rate becomes critical when one wants to predict the outcome of the response and the quality of memory CD8 T cells on a long term (that is, much further than the extent of the experiment). In this case, our analysis showed that depending on the value of the memory cell death rate several scenarii could be envisaged, corresponding either to a sustained or to a slowly decreasing population of CD8 memory T cells.

Based on these conclusions, further experimental investigations should be performed to provide more biological constraints to the parameter space:

1. *Assessing proliferation rates.*

   Cell rates can be experimentally tracked using CFSE and viability dyes [43, 44, 45, 46]. CFSE allows to determine the number of cells having performed a given number of divisions (up to 7/8) at one given time. Thus, a kinetics follow-up with CFSE can be used to derive the proliferation rates of effector cells [47]. One difficulty lies within the fact that most cell cycle models (allowing to extract relevant cycle values from labeling data) are well fitted for *in vitro* data, but analyzing *in vivo* data will be somewhat more challenging.

2. *Assessing death rates.*

   As mentioned earlier, an experimental investigation of CD8 T cell death rate by apoptosis along the resolution of the infection would be very helpful. Similarly to what would be done for estimating proliferation rates, a kinetics of the number of dead cells identified by viability dyes can lead to effector cell death rate estimation, which can also be derived from CFSE

dilution models. The main difficulty here lies within the fact that apoptotic cells are very rapidly eliminated *in vivo*, and therefore the actual death rate will tend to be underestimated.

3. *Assessing CD8 T cell subpopulation kinetics.*

   Estimation of parameter values has been mainly based on the simulation of the total CD8 T cell population kinetics, even though the model provides dynamics for all CD8 T cell subpopulations (naive, effector and memory cell populations). A notable exception is the use of the population of memory CD8 T cells in the last section to derive predictions of the model in terms of memory cell sustainability. Yet, fitting not only the total CD8 T cell population count, but also the subpopulation kinetics should be a relevant method to obtain more information on model parameters. One may note that our identification of pathogen-specific parameters relies on the Naive to Effector to Memory cells differentiation pathway, and could possibly change if alternative differentiation pathways are to be used, based on the identification of relevant markers. This study about subpopulation kinetics is currently under investigation: it is not a trivial experimental task to distinguish unequivocally, at every time of the response and in particular during the peak of the response, the different populations of naive, effector and memory cells. In particular, we still lack markers or combinations of markers that are uniquely expressed by these different CD8 T cell differentiation states. For instance, while the percentage of CD127+ cells comes to a nadir during the expansion phase, CD127+ CD8 T cell counts still increase and contract through the response (data not shown), making it difficult to exclude the possibility that CD127+ memory cells may be the progeny of CD127+ effector cells and not of CD127- effectors, as commonly accepted (the classification based on CD62L and CD27, used for instance in [48], is also still a matter of debate). We are currently working on establishing more relevant combinations of markers that would permit to generate the kinetics of subpopulations during the response.

4. *Assessing pathogen kinetics.*

   Confronting the simulated pathogen kinetics to experimental pathogen kinetics could also help validating model parameters. For influenza infection, experimental data available in the literature suggest that the viral dynamics mainly occur in the first 10 days post-infection [49, 50, 51, 52]. Wolk et al. [49] and Sun et al. [52] obtained experimental dynamics where the virus titer tends to increase until a peak (around day 3), then decreases. This behavior is similar to what we obtained for the pathogen kinetics in the model (see Supp. Fig. 5), even though this behavior is more visible for Flu and *Lm* than for VV. Measuring viruses or bacteria counts would only be an indirect reflect of the "pathogen" in our model, where this term encompasses pathogen counts and its uptake, processing and presentation by APCs.

Altogether, our analysis stresses that differences observed in the three CD8 T cell responses could be explained by a limited number of parameters, and that these parameters could allow identifying either the pathogen responsible for the infection or the nature of the pathogen. Indeed, it is possible that differences observed according to the considered pathogen are due to the route of infection, but they can also be due to other aspects that have not been taken into account in this modeling approach: different pathogens can for instance induce different inflammatory responses [42], or different CD4 responses [53]. As mentioned above, different inflammatory contexts influence the quantity and quality of effector cells [42], which may translate in different effector-induced death rates and effector proliferation rates in our immunization protocols. Different CD4 responses can affect the activation of naive CD8 T cells (by helping antigen-presenting cells) and the generation of memory cells [53], potentially affecting the differentiation rates in effector and memory cells. Such

influences can be what we observe as different values of some key parameters. A systemic infection with vaccinia could be induced through intravenous injection, in order to determine whether the differences observed between the three different data series are due to the nature of the pathogen or to the route of infection. Our modeling approach and method of parameter values estimation therefore paves the way for future studies aiming at building a predictive model of the immune response, and highlights the need for an experimental validation of some parameter values at different steps before increasing models complexity.

4 Methods

4.1 Experimental work

Experiments were performed to measure the CD8 T cell responses to the three pathogens in vivo. CD8 T cell numbers were measured by flow cytometry during the course of the immune response that was triggered by infection. All experimental procedures were approved by our local ethics committee (CECCAPP (Comité d'Evaluation Commun au Centre Léon Bérard, à l'Animalerie de transit de l'ENS, au PBES et au laboratoire P4)) and accreditations have been obtained from French governmental agencies.

CD8 T cells from CD45.1+ F5 TCR transgenic mice (B6.SJL-Ptprc[a] Pepc[b]/BoyCrl-Tg(CD2-TcraF5,CD2-Tcrb F5)1Kio/Jmar) recognizing the NP68 epitope were transferred by retro-orbital injection in congenic CD45.2+ C57Bl/6 mice (C57BL6/J). To normalize the experiments the same number of naive F5 CD8 T cells (2.10^5) were transferred in the three models of infection. The initial value of naive cells that grafted in the host was experimentally measured in the influenza experiment, and since the same number of F5 TCR transgenic T cells was used for all experiments, the same initial value was assumed for experiments with vaccinia and *Listeria*.

The influenza H1N1 WSN strain, the vaccinia WR strain and the *Listeria* 10403s strain were all modified by reverse genetics to express the NP68 epitope. H1N1-NP was constructed and produced by Drs. O. Ferraris and M. Ottmann in Pr. B. Lina's laboratory [54]. VV-NP was constructed and produced by Dr. D.Y.L. Teoh in Pr. Sir A.J. McMichael's laboratory [55]. *Lm*-NP was constructed and produced by Dr. B. Mercier in Drs. N. Bonnefoy-Berard and G. Lauvau's laboratories (unpublished data). In three distinct experiments, mice were inoculated intranasaly with (2.10^5 TCID$_{50}$) H1N1-NP or (2.10^5 PFU) VV-NP or intravenously with 3000 *Lm*-NP bacteria, the day after the transfer of naive F5 CD8 T cells. Intranasal inoculation of the influenza or the vaccinia viruses leads to a localized infection of the lung, while intravenous inoculation of *Listeria* leads to a systemic infection of the host. Mice were briefly anesthetized with 3% isofluorane in an oxygen chamber before being transferred or infected intravenously with *Lm*-NP or profoundly anesthetized with 70 mg/kg of Ketamin and 9 mg/kg of Xylazin before intranasal infection with viruses.

For each experiment a cohort of 20 mice was used, alternate groups of 5 mice were bled at regular intervals to quantify F5 CD8 T cell numbers. Mice blood was sampled, at days 0, 3, 4, 5, 6, 10, 12, 14, 18, 21, 28, 38 post-infection for experiment with H1N1-NP, at days 4, 6, 7, 8, 11, 13, 15, 19, 22, 28, 35, 47 for experiment with VV-NP, and at days 3, 5, 7, 10, 12, 17, 34 for experiment with *Lm*-NP. The time course was designed in order to capture the different phases of the response, i.e. the activation-induced expansion, contraction and memory phases. Cellular expansion was measured in the blood through which CD8 T cell recirculate, wherever their expansion has occurred, allowing us not to model re-circulation between different lymphoid compartments [56]. Analysis of the blood compartment may explain the initial drop in CD8 T cell counts observed (Figure 1), as activated T cells could be retained in the lymphoid organs during the first steps of activation [57].

The volume of blood samples was measured to calculate CD8 T cell numbers and a given number

of fluorescent calibration beads was added to each samples. Cells were then stained with fluorescent antibodies against CD8, CD45 and CD45.1 to identify the transferred F5 CD8 T cells. Samples were then analyzed by flow cytometry to detect F5 CD8 T cells and fluorescent beads. These calibration beads were used to re-calculate the concentration of F5 CD8 T cells per mL of blood and total numbers of circulating F5 CD8 T cells were calculated, considering 2mL of blood per mouse.

Experimental data are freely available upon request to J. Marvel.

4.2 Model

Mice were infected by three live pathogens that can replicate within the host. When they encounter their cognate peptide, naive CD8 T cells are activated and differentiate into effector cells able to eliminate the pathogen, and a fraction of these cells will then differentiate into memory cells (see Figure 2). Ordinary differential equations were used to describe the evolution of CD8 T cell numbers (naive, effector and memory cells), and of the pathogen count. The system of 4 equations includes 4 feedback functions, as cell differentiation, proliferation and death are strongly controlled by feedback loops, depending on interactions between the different CD8 populations (naive, effector, memory cell populations) and with the pathogen. For example, pathogen induces differentiation of naive cells into effector cells, and promotes proliferation of effector cells [14].

Denote by N, E, and M the numbers of naive, effector, and memory CD8 T cells, respectively, and by P the amount of pathogen presented by APCs to CD8 T cells. These quantities evolve according to the following system,

$$\begin{cases} N' &= -\mu_N N - \delta_{NE} PN, \\ E' &= \delta_{NE} PN + \rho_E PE - \mu_E E^2 - \delta_{EM} E, \\ M' &= -\mu_M M + \delta_{EM} E, \\ P' &= \rho_P P^2 - \mu_P EP - \mu_P^0 P, \end{cases} \tag{1}$$

with $N(0) = N_0$, $E(0) = E_0$, $M(0) = M_0$, and $P(0) = P_0$. Naive and memory cells are assumed to die with constant rates μ_N and μ_M, respectively. Naive cells differentiate into effector cells by interacting with pathogens [14] and δ_{NE} denotes the interaction constant. Effector cells proliferate with a rate $\rho_E P$ depending on the pathogen count [10, 14, 15], die by apoptosis with a rate $\mu_E E$ depending on the number of effector cells, due particularly to competition for limited resources such as cytokines or fratricidal death [15, 58], and differentiate in memory cells with a constant rate δ_{EM}. The pathogen is assumed to positively influence its own proliferation with a characteristic constant ρ_P, and it is eliminated with a rate $\mu_P E + \mu_P^0$, where μ_P^0 stands for the natural death rate of the pathogen whereas $\mu_P E$ is an effector cell-dependent death rate [11].

No production of naive cells from hematopoietic stem cells is considered, as naive cells used in the experiments are exogenous and do not self renew in mice (see the previous section).

The model is eventually formed with 9 constant parameters (μ_N, δ_{NE}, ρ_E, μ_E, δ_{EM}, μ_M, ρ_P, μ_P, μ_P^0) and 4 initial conditions (N_0, E_0, M_0 and P_0) that have to be assigned a value. The values of N_0, E_0, and M_0 are known from experimental data: a given amount of purified naive CD8 T cells is injected at time $t = -1$ day in mice, and a number N_0 is assumed to be grafted at time $t = 0$; in the absence of pathogen before $t = 0$ there is no effector or memory cells, so $E_0 = 0$ and $M_0 = 0$. However the value of P_0 is not known, because dynamics of pathogen counts remain unknown in experimental data. Hence, P_0 should be counted as an additional parameter to be determined, and the model would exhibit 10 free parameters. To avoid this additional difficulty, system (1) is scaled

by defining $P \rightsquigarrow P/P_0$, this leads to

$$
\begin{cases}
N' & = & -\mu_N N - \bar{\delta}_{NE} PN, \\
E' & = & \bar{\delta}_{NE} PN + \bar{\rho}_E PE - \mu_E E^2 - \delta_{EM} E, \\
M' & = & -\mu_M M + \delta_{EM} E, \\
P' & = & \bar{\rho}_P P^2 - \mu_P EP - \mu_P^0 P,
\end{cases}
\tag{2}
$$

with $N(0) = N_0$, $E(0) = E_0$, $M(0) = M_0$, and $P(0) = 1$, where for the sake of simplicity, we still denote the pathogen count by P, and $\bar{\delta}_{NE} := \delta_{NE} P_0$, $\bar{\rho}_E := \rho_E P_0$, $\bar{\rho}_P := \rho_P P_0$. Consequently, the parameters $\bar{\delta}_{NE}, \bar{\rho}_E, \bar{\rho}_P$ have not the same meaning as in system (1). However, this does not influence the method to estimate all the parameters, so it does not add any difficulty, and for the sake of simplicity, we omitted the bars on the constant parameters and kept using the notations δ_{NE}, ρ_E, ρ_P in Section 2.

4.3 Identifiabilty of Parameter Values

Inspired by Raue et al. [38, Section 2.3], we define *identifiability* as follows: a model parameter is identifiable if the confidence interval of its estimate is finite. For nonnegative parameters, a confidence interval equal to $[0, +\infty)$ implies non-identifiability. A model is said identifiable if all its parameters are identifiable, and non-identifiable if at least one parameter is not identifiable. Identifiability allows to be confident on parameter values that allow to describe experimental data, even though some parameters may be identifiable and some may be non-identifiable.

Using PottersWheel fitting toolbox [59], we investigated the identifiability of our model parameters. Profile likelihood-based confidence intervals show that for the 3 infections all parameters are non-identifiable (see Supp. Table 1) due to confidence intervals equal to $[0, +\infty)$.

Non-identifiability of the model parameters implies that a correct reproduction of experimental data cannot be associated to a unique parameter value. Consequently, it is meaningless to focus on determining the *best* parameter values reproducing each kinetics of infection.

4.4 Simulations and Selection of Parameter Sets

An exhaustive exploration of the parameter value space was performed, by computing solutions of system (2) using several distinct values for each of the 9 parameters. Since parameter values are not identifiable from experimental data (see previous section) and in order to be as exhaustive as possible, no a priori knowledge of parameter values was considered to determine which values should be preferentially tested. Tested parameter values were only chosen under the constraint of taking into account as much as possible known biological metrics (Table 3), even if some values may look extreme: the goal of this exhaustive parameter estimation remains to investigate as large a range of parameter values as possible, and this idea of systematic parameter sweep leads to considering large intervals of values. The range for each parameter value was determined under these conditions and five values distributed in the interval were tested simultaneously (see Table 3). Numerous preliminary trials (data not shown) were run to determine the five most relevant values for each parameter, resulting in 5^9 parameter value sets, that is to say $1,953,125$ simulations.

One may note that this study focuses on determining parameter values, which are constant, yet it must be kept in mind that some parameters are associated with *non-constant* biological rates. This point is illustrated in Supp. Table 2.

Simulations were performed using facilities of the Calculus Center of the National Institute of Nuclear Physics and Particle Physics (IN2P3). The 250 cores of the IN2P3 were used to distribute

Table 3: **Parameter values used when performing simulations.** To have an idea of the biological meaning of these values, one can consider the following examples of parameter values associated with a death rate, a differentiation rate and a proliferation rate, by keeping in mind that for a population $y(t)$ characterized by a growth rate k (which can be negative when, for instance, the population only dies) one gets $y(t) = y(0) \exp(kt)$, so for instance $y(t = 1 \text{ d}) = y(0) \exp(k)$. When $\mu_M = 10^{-5}$ d^{-1}, it corresponds to the death of almost no (0.001%) memory CD8 T cells per day, and when $\mu_N = 5$ d^{-1} it corresponds to the death of 99.3% of naive cells per day. When $\delta_{NE} = 10^{-3}$ d^{-1}, it corresponds to the differentiation of 0.1% of naive cells in effector cells per day, and when $\delta_{NE} = 0.1$ d^{-1}, it corresponds to the differentiation of 10% of naive cells in effector cells per day. When $\rho_E = 1$ d^{-1}, it corresponds to 1.4 division of an effector cell per day (1 division every 17 hours), and when $\rho_E = 4$ d^{-1}, it corresponds to almost 6 divisions of an effector cell per day (1 division every 4 hours). Parameters μ_E and μ_P (cell^{-1}.d^{-1}) do not directly correspond to cell rates, so their biological meaning is more difficult to define (see Supp. Table 2).

Biological rate (unit)	Param.	Tested values				
Naive cells death rate (d^{-1})	μ_N	0.01	0.1	1	5	10
Naive cells differentiation rate (d^{-1})	δ_{NE}	10^{-3}	5.10^{-3}	0.01	0.05	0.1
Effector cells proliferation rate (d^{-1})	ρ_E	1	1.5	2	3	4
Effector cells death rate (cell^{-1}.d^{-1})	μ_E	10^{-8}	10^{-7}	10^{-6}	10^{-5}	10^{-4}
Effector cells differentiation rate (d^{-1})	δ_{EM}	10^{-5}	10^{-4}	10^{-3}	0.01	0.1
Memory cells death rate (d^{-1})	μ_M	0	10^{-5}	10^{-3}	0.01	0.1
Pathogen effector-cell-dependent death rate (cell^{-1}.d^{-1})	μ_P	10^{-8}	10^{-7}	10^{-6}	10^{-5}	10^{-4}
Pathogen natural death rate (d^{-1})	μ_P^0	10^{-4}	10^{-3}	5.10^{-3}	0.01	0.1
Pathogen proliferation rate (d^{-1})	ρ_P	10^{-4}	10^{-3}	0.01	0.1	1

the large number of simulations, with $7,812$ simulations per core for 249 cores, and $7,937$ simulations for the last core.

The Shapiro-Wilk normality test (using a Bonferroni correction) showed that experimental data are not normally distributed. Indeed, only experimental data associated with Flu infection are not normally distributed, the hypothesis of a normal distribution on day 14 post-infection being rejected with a *p-value*=0.001. Yet, experimental data are log-normally distributed (data not shown). We therefore use the logarithm of experimental data, for the three infections, to perform a comparison with simulated solutions. For each simulation, the error $RSS(x)$ between the experimental mean x_i (the geometrical mean of measured experimental values) measured at time t_i and the corresponding simulated point $x(t_i)$ was determined using a weighted least-square method, with the formula (σ_i denotes the standard deviation associated with the mean x_i)

$$RSS(x) = \sqrt{\sum_i \left(\frac{x_i - x(t_i)}{\sigma_i} \right)^2}.$$

Since the model is based on the description of the dynamics of CD8 T cell subpopulations (naive, effector and memory cells), whereas experimental data correspond to a total CD8 T cell population count, the value of each simulated point $x(t)$ is equal to $log(N(t) + E(t) + M(t))$. All these computed errors were ranked in increasing order. Hence, the smallest errors correspond to the best results and one can focus on the corresponding parameter value sets. One must note that it is not relevant to compare error values between experiments (influenza, vaccinia and *Listeria*), as only rank of errors

is relevant.

The next step is to determine the parameter sets that would be used for a comparison study between the three infections. We defined a parameter set S as "acceptable" if it corresponds to a solution x_S that has values inside the error bars, that is satisfying

$$|x_S(t_i) - x_i| \leq \sigma_i, \quad \text{for all } i \in \{1, \dots, n\}$$

where n denotes the number of experimental points (the experimental cell count at $t = 0$ is not considered, because it is used as an initial condition for the three experiments; consequently, $n = 11$ for Flu infection, $n = 12$ for vaccinia infection, and $n = 7$ for Lm infection). Using this condition, an acceptable parameter set is then a parameter set S such that

$$RSS(x_S) \leq RSS_T := n.$$

Let define $\{S\}$ the number of parameter sets satisfying $RSS(x_S) \leq RSS_T$. For each infection, we finally consider among the $\{S\}$ acceptable parameter sets only the ones associated with a CD8 T cell count mainly composed with memory cells at the end of the experiment/simulation. This is expected from a biological point of view, the population of CD8 T cells being mainly, if not exclusively, composed of memory cells once the infection is resolved. This condition corresponds to parameter sets S such that

$$RSS(x_S) \leq n \text{ and } M_S(t_{end}) > E_S(t_{end}),$$

where t_{end} is the last experimental time point ($t_{end} = 38$ days for Flu infection, $t_{end} = 47$ days for vaccinia infection, and $t_{end} = 34$ days for Lm infection). For each infection, parameter value sets satisfying the above two conditions will be referred to as "acceptable parameter value sets".

Competing interests

The authors declare that they have no competing interests.

Author's contributions

ET performed the model construction and parameter estimation as well as parameter value analysis, together with FC and OG.
ILM, JuM, SD, TA, BM participated in the acquisition of the in vivo data.
GK participated in the parameter estimation process.
FC, CA, JaM, ET and OG conceived the study, and participated in its design and coordination.
FC, ET and OG wrote the manuscript, with the help of JaM and CA.
All authors read and approved the final manuscript.

Acknowledgements

References

[1] F. Ennis, Q. Yi-Hua, D. Riley, A. Rook, G. Schild, R. Pratt, C. Potter, HLA-Restricted Virus-Specific Cytotoxic T-Lymphocyte Responses to Live and Inactivated Influenza Vaccines, J. Theor. Biol. 167 (1994) 323–360.

[2] P. Wong, E. Pamer, CD8 T cell responses to infectious pathogens, Annual review of immunology 21 (2003) 29–70.

[3] K. Kedzierska, N. L. Gruta, S. Turner, P. Doherty, Establishment and recall of CD8+ T-cell memory in a model of localized transient infection, Immunol. reviews 211 (2006) 133–145.

[4] J. Snyder, I. Belyakov, A. Dzutsev, F. Lemonnier, J. Berzofsky, Protection against Lethal Vaccinia Virus Challenge in HLA-A2 Transgenic Mice by Immunization with a Single CD8 T-Cell Peptide Epitope of Vaccinia and Variola Viruses, J. Virol. 180 (2004) 7052–7060.

[5] L. Jing, T. Chong, B. Byrd, C. McClurkan, J. Huang, B. Story, K. Dunkley, L. Aldaz-Carroll, R. Eisenberg, G. Cohen, W. Kwok, A. Sette, D. Koelle, Dominance and diversity in the primary human CD4 T cell response to replication-competent vaccinia virus, J. Immunol. 178 (2007) 6374–6386.

[6] D. Busch, E. Pamer, T lymphocyte dynamics during Listeria monocytogenes infection, Immunology letters 65 (1999) 93–98.

[7] K. Murali-Krishna, J. Altman, M.Suresh, D. Sourdive, A. Zajax, J. Miller, J. Slansky, R. Ahmed, Counting Antigen-Specific CD8 T Cells: a Reevaluation of Bystander Activation during Viral Infection, Immunity 8 (1998) 177–187.

[8] R. De Boer, M. Oprea, R. Antia, K. Murali-Krishna, R. Ahmed, A. Perelson, Recruitment Times, Proliferation, and Apoptosis Rates during the CD8 T-Cell Response to Lymphocytic Choriomeningitis Virus, J. Virol. (2001) 10663–10669.

[9] I. Rouzine, K. Murali-Krishna, R. Ahmed, Generals die in friendly fire, or modeling immune response to HIV, J. Computational and Appl. Math. 184 (2005) 258–274.

[10] P. Kim, P. Lee, D. Levy, Modeling regulation mechanisms in the immune system, J. Theor. Biol. 246 (2007) 33–69.

[11] R. Antia, C. Bergstrom, S. Pilyugin, S. Kaech, R. Ahmed, Models of CD8+ Responses: 1. What is the Antigen-independent Proliferation Program, J. Theor. Biol. 221 (2003) 585–598.

[12] R. Antia, V. Ganusov, R. Ahmed, The role of models in understanding CD8$^+$ T-cell memory, Nat. Reviews 5 (2005) 101–111.

[13] E. Terry, J. Marvel, C. Arpin, O. Gandrillon, F. Crauste, Mathematical Model of the primary CD8 T Cell Immune Response: Stability Analysis of a Nonlinear Age-Structured System, J. Math. Bio. 65 (2012) 263–291.

[14] V. Appay, S. Rowland-Jones, Lessons from the study of T-cell differentiation in persistent human virus infection, Seminars in Immunol. 16 (2004) 205–212.

[15] R. Kemp, T. Powell, D. Dwyer, R. Dutton, Cutting Edge: Regulation of CD8$^+$ T Cell Effector Population Size, J. Immunol. 173 (2004) 2923–2927.

[16] Z. Jin, J. Zhang, L.-P. Song, G.-Q. Sun, J. Kan, H. Zhu, Modelling and analysis of inluenza A (H1N1) on networks, BMC Public Health 11(Suppl 1):S9.

[17] H. Lee, D. Topham, S. Park, J. Hollenbaugh, J. Treanor, T. Mosmann, X. Jin, B. Ward, H. Miao, J. Holden-Wiltse, A. Perelson, M. Zand, H. Wu, Simulation and Prediction of the Adaptive Immune Response to Influenza A Virus Infection, J. Virol. 83 (2009) 7151–7165.

[18] R. Parker, L. Bronson, R. Green, Further studies of the infectious unit of vaccinia, The Journal of experimental medicine 74 (1941) 263–281.

[19] C. Oseroff, B. Peters, V. Pasquetto, M. Moutaftsi, J. Sidney, V. Panchanathan, D. Tscharke, B. Maillere, H. Grey, A. Sette, Dissociation between epitope hierarchy and immunoprevalence in CD8 responses to vaccinia virus western reserve, J. Immunol. 180 (2008) 7193–7202.

[20] K. Rehm, R. Connor, G. Jones, K. Yimbu, M. Mannie, R. Roper, Vaccinia virus decreases major histocompatibility complex (MHC) class II antigen presentation, T-cell priming, and peptide association with MHC class II, Immunology 128 (2009) 381–392.

[21] J. Lantto, M. H. Hansen, S. Rasmussen, L. Steinaa, T. Poulsen, J. Duggan, M. Dennis, I. Naylor, L. Easterbrook, S. Bregenholt, J. Haurum, A. Jensen, Capturing the natural diversity of the human antibody response against vaccinia virus, J. Virol. 85 (2011) 1820–1833.

[22] E. Pamer, Immune responses to Listeria monocytogenes, Nature Reviews Immunology 4 (2004) 812–823.

[23] A. Smith, R. Ribeiro, Modeling the Viral Dynamics of Influenza A Virus Infection, Immunology 30(3) (2010) 291–298.

[24] C. Beauchemin, A. Handel, A review of mathematical models of influenza A infections within a host or cell culture: lessons learned and challenges ahead, BMC Public Health 11(Suppl 1):S7.

[25] M. Alexander, R. Kobes, Effects of vaccination and population structure on influenza epidemic spread in the presence of two circulating strains, BMC Public Health 11(Suppl 1):S8.

[26] G. Bocharov, A. Romanyukha, Mathematical Model of Antiviral Immune Response III. Influenza A Virus Infection, J. Theor. Biol. 167 (1994) 323–360.

[27] C. Beauchemin, J. Samuel, J. Tuszynskia, A simple cellular automaton model for influenza A viral infections, J. Theor. Biol. 232 (2005) 223–234.

[28] C. Beauchemin, Probing the Effects of the Well-mixed Assumption on Viral Infection Dynamics, J. Theor. Biol. 242(2) (2006) 464–477.

[29] P. Baccam, C. Beauchemin, C. Macken, F. Hayden, A. Perelson, Kinetics of Influenza A Virus Infection in Humans, J. Virol. 80 (2006) 7590–7599.

[30] C. Beauchemin, J. McSharry, G. Drusano, J. Nguyen, G. Went, R. Ribeiro, A. Perelson, Modeling amantadine treatment of influenza A virus in vitro, J. Theor. Biol. 254 (2008) 439–451.

[31] G. Mercer, S. Barry, H. Kelly, Modelling the effect of seasonal influenza vaccination on the risk of pandemic influenza infection, BMC Public Health 11(Suppl 1):S11.

[32] R. Saenz, M. Quinlivan, D. Elton, S. MacRae, A. Blunden, J. Mumford, J. Daly, P. Digard, A. Cullinane, B. Grenfell, J. McCauley, J. Wood, J. Gog, Dynamics of Influenza Virus Infection and Pathology, J. Virol. 84 (2010) 3974–3983.

[33] D. Chang, C. Young, Simple scaling laws for influenza A rise time, duration, and severity, J. Theor. Biol. 246 (2007) 621–635.

[34] A. Handel, I. Longini, J., R. Antia, Towards a quantitative understanding of the within-host dynamics of influenza A infections, J. R. Soc. Interface 7 (2010) 35–47.

[35] H. Miao, J. Hollenbaugh, M. Zand, J. Holden-Wiltse, T. Mosmann, A. Perelson, H. Wu, D. Topham, Quantifying the Early Immune Response and Adaptive Immune Response Kinetics in Mice Infected with Influenza A Virus, J. Virol. 84 (2010) 6687–6698.

[36] A. Tridane, Y. Kuang, Modeling the interaction of cytotoxic T lymphocytes and influenza virus infected epithelial cells, Math. Biosci. Eng. 7 (2010) 171–185.

[37] B. Hancioglu, D. Swigon, G. Clermont, A dynamical model of human immune response to influenza A virus infection, J. Virol. 83 (2009) 7151–7165.

[38] A. Raue, C. Kreutz, T. Maiwald, J. Bachmann, M. Schilling, U. Klingmuller, J. Timmer, Structural and practical identifiability analysis of partially observed dynamical models by exploiting the profile likelihood, Bioinformatics 25 (2009) 1923–1929.

[39] R. De Boer, D. Homann, A. Perelson, Different dynamics of CD4+ and CD8+ T cell responses during and after acute lymphocytic choriomeningitis virus infection, J. Immunol. 171 (2003) 3928–3935.

[40] C. Althaus, V. Ganusov, R. De Boer, Dynamics of CD8 T Cell Responses during Acute and Chronic Lymphocytic Choriomeningitis Virus Infection, J. Immunol. 179 (2007) 2944–2951.

[41] V. Ganusov, Discriminating between different pathways of memory CD8+ T cell differentiation, J. Immunol. 179 (2007) 5006–5013.

[42] S. Condotta, M. Richer, V. Badovinac, J. Harty, Probing CD8 T cell responses with Listeria monocytogenes infection, Adv Immunol 113 (2012) 51–80.

[43] R. Nordon, M. Nakamura, C. Ramirez, R. Odell, Analysis of growth kinetics by division tracking, Immunol. and cell biol. 77 (1999) 523–529.

[44] S. Bernard, L. Pujo-Menjouet, M. Mackey, Analysis of cell kinetics using a cell division marker: mathematical modeling of experimental data, Biophysical journal 84 (2003) 3414–3424.

[45] R. De Boer, A. Perelson, Estimating division and death rates from CFSE data, Journal of computational and applied mathematics 184 (2005) 140–164.

[46] R. De Boer, V. Ganusov, D. Milutinović, P. Hodgkin, A. Perelson, Estimating lymphocyte division and death rates from CFSE data, Bulletin of mathematical biology 68 (2006) 1011–1031.

[47] R. De Boer, A. Perelson, Quantifying T lymphocyte turnover, J. Theor. Biol. 327 (2013) 45–87.

[48] V. Buchholz, M. Flossdorf, I. Hensel, L. Kretschmer, B. Weissbrich, P. Gräf, A. Verschoor, M. Schiemann, T. Höfer, D. Busch, Disparate individual fates compose robust CD8+ T cell immunity, Science 340 (2013) 630–5.

[49] K. Wolk, E. Lazarowski, Z. Traylor, N. Erin, N. Jewell, R. Durbin, J. Durbin, I. Davis, Influenza A virus inhibits alveolar fluid clearance in BALB/c mice, American journal of respiratory and critical care medicine 178 (2008) 969–976.

[50] E. Desmet, J. Hollenbaugh, P. Sime, T. Wright, D. Topham, A. Sant, T. Takimoto, S. Dewhurst, Mixed Lineage Kinase 3 deficiency delays viral clearance in the lung and is associated with diminished influenza-induced cytopathic effect in infected cells, Virology 400 (2010) 224–232.

[51] M. Garigliany, A. Habyarimana, B. Lambrecht, E. V. de Paar, A. Cornet, T. V. D. Berg, D. Desmecht, Influenza A strain-dependent pathogenesis in fatal H1N1 and H5N1 subtype infections of mice, Emerg Infect Dis 16 (2010) 595–603.

[52] S. Sun, G. Zhao, W. Xiao, J. Hu, Y. Guo, H. Yu, X. Wu, Y. Tan, Y. Zhou, Age-related sensitivity and pathological differences in infections by 2009 pandemic influenza A (H1N1) virus, J. Virol. 8 (2011) 52.

[53] W. Cui, S. Kaech, Generation of effector cd8+ t cells and their conversion to memory t cells, Immunol Rev. 236 (2010) 151–166.

[54] V. Jubin, E. Ventre, Y. Leverrier, S. Djebali, K. Mayol, M. Tomkowiak, J. Mafille, M. Teixeira, D. Teoh, B. Lina, T. Walzer, C. Arpin, J. Marvel, T inflammatory memory CD8 T cells participate to antiviral response and generate secondary memory cells with an advantage in XCL1 production, Immunol. Research 52 (2012) 284–293.

[55] A. Cottalorda, B. Mercier, F. Mbitikon-Kobo, C. Arpin, D. Teoh, A. McMichael, J. Marvel, N. Bonnefoy-Berard, TLR2 engagement on memory CD8+ T cells improves their cytokine-mediated proliferation and IFN-γ secretion in the absence of Ag, Eur. J. Immunol. 39 (2009) 2673–2681.

[56] H. Wu, A. Kumar, H. Miao, J. Holden-Wiltse, T. Mosmann, A. Livingstone, G. Belz, A. Perelson, M. Zand, D. Topham, Modeling of Influenza-Specific CD8+ T Cells during the Primary Response Indicates that the Spleen Is a Major Source of Effectors, J. Immunol. 187 (2011) 4474–4482.

[57] S. Hugues, L. Fetler, L. Bonifaz, J. Helft, F. Amblard, S. Amigorena, Distinct T cell dynamics in lymph nodes during the induction of tolerance and immunity, Nature Immunol. 5 (2004) 1235–1242.

[58] M. Su, P. Wladen, D. Golan, H. Eisen, Cognate peptide-induced destruction of CD8^{+} cytotoxic T lymphocytes is due to fratricide, J. Immunol. 151 (1993) 658–667.

[59] T. Maiwald, J. Timmer, Dynamical modeling and multi-experiment fitting with potterswheel, Bioinformatics 24 (2008) 2037–2043.